

DFTT 26/94
 DTP/94/46
 December 1994
 Revised July 1995

Intermediate mass standard model Higgs boson at the proposed CERN LEP \otimes LHC ep collider¹

Ghadir Abu Leil^a and Stefano Moretti^{a,b,2}

*a) Department of Physics, University of Durham,
 South Road, Durham DH1 3LE, U.K.*

*b) Dipartimento di Fisica Teorica, Università di Torino,
 and INFN, Sezione di Torino,
 V. Pietro Giuria 1, 10125 Torino, Italy.*

Abstract

The production of the \mathcal{SM} Higgs ϕ with intermediate mass at the proposed CERN LEP \otimes LHC ep collider in $\gamma q(\bar{q}) \rightarrow W^\pm \phi q'(\bar{q}')$, $\gamma q(\bar{q}) \rightarrow Z^0 \phi q(\bar{q})$ and $g\gamma \rightarrow q\bar{q}\phi$ events is studied. This is done for all possible (massive) flavours of the quarks $q(q')$ and using photons generated via Compton back-scattering of laser light. We study signatures in which the Higgs decays to $b\bar{b}$ -pairs and the electroweak vector bosons W^\pm and Z^0 decay either hadronically or leptonically. All possible backgrounds to these signals are also computed. Flavour identification on b -jets is assumed. Explicit formulae for the helicity amplitudes of the above processes are given.

¹Work supported in part by Ministero dell' Università e della Ricerca Scientifica (SM) and by a University of Durham Studentship and a World Lab. Fellowship ICSC (GAL).

²Address after September 1995: Cavendish Laboratory, University of Cambridge, Madingley Road, Cambridge, CB3 0HE, U.K.

Introduction

The Higgs sector is one of the most investigated parts of the Standard Model (\mathcal{SM}) [1, 2], yet continues to be very elusive. So far the Higgs particle has evaded all searches. Nevertheless, a lower limit on the mass of the \mathcal{SM} Higgs ϕ of ≈ 60 GeV was extracted from the lack of $e^+e^- \rightarrow Z^0 \rightarrow Z^{0*}\phi$ events at LEP I [3]. An upper bound of ≈ 1 TeV is expected. This was derived by requiring the validity of perturbation theory [4] and the unitarity of the model [5]. Therefore, if the \mathcal{SM} Higgs ϕ exists, we could expect it to be discovered by the next generation of CERN high energy colliders: LEP II ($\sqrt{s}_{ee} = 160\text{--}200$ GeV) [6] and the LHC ($\sqrt{s}_{pp} = 10, 14$ TeV) [7].

LEP II will be able to cover the mass range $M_\phi < 80\text{--}100$ GeV. A Higgs with a larger mass should be searched for at the LHC. At LEP II ϕ can be detected³ through a large variety of decay channels, the most favoured being $Z^0\phi \rightarrow (\mu^+\mu^-)(b\bar{b})$. A Higgs boson with mass $M_\phi \gtrsim 130$ GeV is clearly detectable at the LHC using the four-lepton mode $\phi \rightarrow Z^0Z^0 \rightarrow \ell\bar{\ell}\ell\bar{\ell}$ ⁴. Due to the QCD backgrounds typical of hadron colliders, it is still controversial whether it is possible to detect an intermediate mass Higgs⁵ in the mass range $90 \lesssim M_\phi \lesssim 130$ GeV (where ϕ mainly decays to $b\bar{b}$ pairs). In this mass range ϕ can be searched for through the rare $\gamma\gamma$ decay mode and this relies on the fact that both a high luminosity and a very high di-photon mass resolution must be achieved at the LHC [15]. It is also unclear whether it is possible to cleanly detect the intermediate \mathcal{SM} Higgs in the $\phi \rightarrow b\bar{b}$ channel using the b -tagging capabilities of vertex detectors [16, 17]. The main difficulties being the expected low signal rates after reconstruction, the necessity to have an accurate control on all the possible background sources and to achieve a very high b -tagging performance [18].

In the distant future, cleaner environments for studying the Higgs boson parameters will be the e^+e^- linear accelerators ($\sqrt{s}_{ee} = 350\text{--}2000$ GeV) [19, 20, 21, 22, 23].

At the Next Linear Collider (NLC), with $\sqrt{s}_{ee} = 300\text{--}500$ GeV [22], the Higgs boson can be searched for through a large number of channels over the whole intermediate mass range [24]. The dominant production mechanism is the Bjorken reaction for \sqrt{s}_{ee} below 500 GeV while the $W^\pm W^\pm$ - and Z^0Z^0 -fusion processes [25] will dominate at larger energies. At $\sqrt{s}_{ee} \gtrsim 500$ GeV [21] a heavy Higgs can be detected in the four-jet modes $\phi \rightarrow W^\pm W^\mp, Z^0Z^0 \rightarrow jjjj$ [26, 27] in addition to the 4ℓ -mode. At higher energies, $\sqrt{s}_{ee} = 1\text{--}2$ TeV [23], the same search strategies still hold with the fusion mechanisms becoming the dominant ones.

The conversion of the linear e^+e^- NLCs into $\gamma\gamma$ and/or $e\gamma$ colliders, by photons generated via Compton back-scattering of laser light, will provide new possibilities for detecting and studying the Higgs boson [28]. In $\gamma\gamma$ collisions two of the important channels will be: the production of a heavy Higgs (up to ≈ 350 GeV) by a triangular loop of heavy fermions or W^\pm , with the detection via the decay mode $\phi \rightarrow Z^0Z^0 \rightarrow q\bar{q}\ell^+\ell^-$ at $\sqrt{s}_{ee} = 500$ GeV [29], and the process $\gamma\gamma \rightarrow t\bar{t}\phi$, which appears more useful than the corresponding e^+e^- one in measuring the top Yukawa coupling $t\phi$, at $\sqrt{s}_{ee} = 1\text{--}2$ TeV [30]. The $e\gamma$ option at linear colliders can be exploited for studying Higgs production via the process $e\gamma \rightarrow \nu_e W\phi$,

³And produced via the Bjorken bremsstrahlung process $e^+e^- \rightarrow Z^{0*} \rightarrow Z^0\phi$ [8].

⁴With ϕ produced via gg - [9] or $W^\pm W^\mp$ - and Z^0Z^0 -fusion [10].

⁵Via the associated production with a W^\pm boson (decaying leptonically to $\ell\nu$) [11, 12] or a $t\bar{t}$ pair (with one t decaying semileptonically to $b\ell\nu$) [13, 14].

at $\sqrt{s}_{ee} = 1 - 2$ TeV and over the mass range $60 \text{ GeV} \lesssim M_\phi \lesssim 150 \text{ GeV}$ [31, 32], using the signature $W^-\phi \rightarrow (jj)(b\bar{b})$ [33]. The cross section for the above process at such \sqrt{s}_{ee} 's is comparable to the fusion process $e^+e^- \rightarrow \bar{\nu}_e\nu_e W^{\pm*}W^{\mp*} \rightarrow \bar{\nu}_e\nu_e\phi$ and larger than the bremsstrahlung reaction $e^+e^- \rightarrow Z^{0*} \rightarrow Z^0\phi$. Finally, it has been shown in ref. [34] that the process $e\gamma \rightarrow e\gamma\gamma \rightarrow e\phi$ is the most important mechanism for ϕ -production at $\sqrt{s}_{ee} = 500$ GeV, for $M_\phi \gtrsim 140$ GeV.

Let us now consider the production of the \mathcal{SM} Higgs boson at ep machines. This seems to be beyond the capabilities of HERA [35], which has been primarily designed for providing accurate data on the proton structure functions in the small- x region, more than for Higgs searches [36]. In the future, another ep collider is contemplated, the CERN LEP \otimes LHC accelerator: it will combine an electron/positron beam from LEP II and a proton beam from the LHC [7, 37]. A detailed study on the detectability of an intermediate mass \mathcal{SM} Higgs boson at such a machine has been presented in ref. [38]. This is based on the $W^\pm W^\mp$ - and $Z^0 Z^0$ -fusion processes [36, 39, 40], with ϕ decaying to $b\bar{b}$. It has been shown that it should be possible to detect ϕ provided that a high luminosity and/or an excellent b -flavour identification can be achieved. Only recently has the possibility of resorting to back-scattered laser photons at the ep CERN collider been suggested [41], searching for, e.g., $\gamma q \rightarrow q'W^\pm\phi$ events, with $\phi \rightarrow b\bar{b}$ and $W^\pm \rightarrow \ell\nu$ or jj , which should give detectable Higgs signals if good $M_{b\bar{b}}$ invariant mass resolution can be achieved and efficient b -tagging can be performed.

The purpose of this paper is to study the following reactions at the LEP \otimes LHC ep collider

$$q\gamma \rightarrow q'W^\pm\phi, \quad (1)$$

$$q\gamma \rightarrow qZ^0\phi, \quad (2)$$

$$g\gamma \rightarrow q\bar{q}\phi, \quad (3)$$

in the intermediate mass range of ϕ , for all possible (anti)flavours of the (anti)quarks $q(q')$, using laser back-scattered photons. We discuss their relevance to the detection of the \mathcal{SM} Higgs and the study of its parameters, with the Higgs decaying to $b\bar{b}$ -pairs and assuming flavour identification on its decay products.

Although process (1) has already been studied in [41], and the part of the analysis devoted to it here largely overlaps that study, we decided nevertheless to include it for completeness and since, in principle, we can slightly improve the results previously obtained. In fact, since we consider heavy quarks we include additional Higgs bremsstrahlung off quarks in the amplitudes, even though these are suppressed with respect to contributions coming from diagrams involving ϕW^+W^- vertices. We also computed all the necessary rates for all the relevant backgrounds exactly, whereas these latter contributions were only estimated in [41]. Reaction (3) has been analysed in [42] for \mathcal{MSSM} neutral Higgses, b -quarks and using bremsstrahlung photons but to our knowledge, neither the larger energy option available at LEP \otimes LHC nor the possibility of using laser back-scattered photons has been exploited.

There are at least two important motivations for analysing processes (1)–(3) at the LEP \otimes LHC collider. First, if the \mathcal{SM} Higgs boson turns out to have an intermediate mass greater than the maximum value that can be reached by LEP II and if the LHC detectors are not able to achieve the necessary performances for the predicted Higgs measurements [18], the ep CERN collider will be the first alternative option available for studying such a Higgs,

as it will certainly be operating before any NLC. Second, although both the cross sections and the luminosity at LEP \otimes LHC are expected to be small if compared with the LHC ones, the CERN ep option will constitute the first TeV energy environment partially free from the enormous QCD background typical of purely hadronic colliders. Moreover, processes (1)–(3) have the advantage, compared to the $W^\pm W^{\mp}$ and $Z^0 Z^0$ –fusion mechanisms, that the additional heavy particles W^\pm and Z^0 (and also t , in principle) can be used for tagging purposes by searching for their decays, thus increasing the signal to background ratio.

The plan of the paper is as follows. In Section II we give details of the calculation and the numerical values adopted for the various parameters. Section III is devoted to the discussion of the results, while the conclusions are in Section IV. The helicity amplitudes for processes (1)–(3) are presented in the Appendix.

Calculation

Fig. 1 shows all the Feynman diagrams at tree level contributing to the reactions (1) and (2) in the unitary gauge, where (q, q', V) represent the possible combinations (d, u, W^-) , (u, d, W^+) and (q, q, Z^0) respectively (in the case of process (2) only the first eight diagrams of fig. 1 contribute). Fig. 2 shows the Feynman diagrams at tree level for process (3). All quarks have been considered massive, so diagrams with a direct coupling of ϕ to the fermion lines have been taken into account.

The amplitudes squared have been computed by means of the spinor techniques of refs. [43, 44] and, as a check, also by the method of ref. [45]. The matrix elements for the processes $\bar{d}\gamma \rightarrow \bar{u}W^+\phi$ / $\bar{u}\gamma \rightarrow \bar{d}W^-\phi$ and $\bar{q}\gamma \rightarrow \bar{q}Z^0\phi$ can easily be obtained by trivial operations of charge–conjugation. All of the above amplitudes have been tested for gauge invariance. We were also able to “roughly”⁶ reproduce, with appropriate couplings, hadron distributions and luminosity function of the photons, the results of ref. [41] and of ref. [42]. Moreover, since a simple adaptation of the implemented formulae (by changing photon couplings from quarks into leptons and setting the quark masses equal to zero) allowed us to reproduce the computation of ref. [33], we have checked our helicity amplitudes in this way also.

As proton structure functions we adopted the HMRS set B [46] (this was done in order to make comparisons with already published work easier), setting the energy scale equal to the center–of–mass (CM) energy at the parton level (i.e. $\mu = \sqrt{\hat{s}}_{\text{parton}}$). The strong coupling constant α_s , which appears in the gluon initiated processes, has been evaluated at two loops, for $\Lambda_{QCD} = 190$ MeV, with a number $N_f = 5$ of active flavours and a scale μ equal to that used for the proton structure functions. We are confident that changing the energy scale and/or distribution function choice should not affect our results by more than a factor of two⁷.

For the energy spectrum of the back–scattered (unpolarized) photon we have used [49]

$$F_{\gamma/e}(x) = \frac{1}{D(\xi)} \left[1 - x + \frac{1}{1-x} - \frac{4x}{\xi(1-x)} + \frac{4x^2}{\xi^2(1-x)^2} \right], \quad (4)$$

⁶See footnote 9 below.

⁷We verified this in few cases by comparing the actual results to the ones obtained from the more recent set of structure functions MRS(A) [47].

where $D(\xi)$ is the normalisation factor

$$D(\xi) = \left(1 - \frac{4}{\xi} - \frac{8}{\xi^2}\right) \ln(1 + \xi) + \frac{1}{2} + \frac{8}{\xi} - \frac{1}{2(1 + \xi)^2}, \quad (5)$$

and $\xi = 4E_0\omega_0/m_e^2$, ω_0 is the incoming laser photon energy and E_0 the (unpolarized) electron/positron energy. In eq. (4) $x = \omega/E_0$ is the fraction of the energy of the incident electron/positron carried by the back-scattered photon, with a maximum value

$$x_{\max} = \frac{\xi}{1 + \xi}. \quad (6)$$

In order to maximise ω while avoiding e^+e^- pair creation, one takes ω_0 such that $\xi = 2(1 + \sqrt{2})$ and one gets the typical values $\xi \simeq 4.8$, $x_{\max} \simeq 0.83$, $D(\xi) \simeq 1.8$.

In the case of $q(g)\gamma$ scattering from ep collisions, the total cross section σ is obtained by folding the subprocess cross section $\hat{\sigma}$ with the photon $F_{\gamma/e}$ and hadron $F_{q(g)/p}$ luminosities:

$$\sigma(s_{ep}) = \int_{x_{\min}^\gamma}^{x_{\max}^\gamma} dx^\gamma \int_{x_{\min}^{q(g)}}^{1-x^\gamma} dx^{q(g)} F_{\gamma/e}(x^\gamma) F_{q(g)/p}(x^{q(g)}) \hat{\sigma}(\hat{s}_{q(g)\gamma} = x^\gamma x^{q(g)} s_{ep}), \quad (7)$$

where $\hat{s}_{q(g)\gamma}$ is the CM energy at parton (i.e., $q(g)\gamma$) level, while

$$x_{\min}^\gamma x_{\min}^{q(g)} = \frac{(M_{\text{final}})^2}{s_{ep}}, \quad (8)$$

where M_{final} is the sum of the final state particle masses.

The multidimensional integrations have been performed numerically using the Monte Carlo routine VEGAS [48].

To our knowledge, a detailed study, as for the cases of $e\gamma$ and $\gamma\gamma$ collisions [49], on the efficiency of the laser back-scattering method in converting $e \rightarrow \gamma$ at ep colliders does not exist. In this paper we assume for the effective γp luminosity the same as the ep one, therefore the conversion efficiency of electrons into backscattered γ 's is one. For the discussion of the results we have adopted an overall total integrated luminosity $\mathcal{L} = 3 \text{ fb}^{-1}$ per year, the value of ref. [41].

For the numerical part of our work, we have taken $\alpha_{em} = 1/128$ and $\sin^2 \theta_W \equiv s_W^2 = 0.23$, while for the gauge boson masses and widths: $M_{Z^0} = 91.175 \text{ GeV}$, $\Gamma_{Z^0} = 2.5 \text{ GeV}$, $M_{W^\pm} = M_{Z^0} \cos \theta_W \equiv M_{Z^0} c_W$ and $\Gamma_{W^\pm} = 2.2 \text{ GeV}$. For the fermions we have: $m_e = 0.511 \times 10^{-3} \text{ GeV}$, $m_\mu = 0.105 \text{ GeV}$, $m_\tau = 1.78 \text{ GeV}$, $m_u = 8.0 \times 10^{-3} \text{ GeV}$, $m_d = 15.0 \times 10^{-3} \text{ GeV}$, $m_s = 0.3 \text{ GeV}$, $m_c = 1.7 \text{ GeV}$, $m_b = 5.0 \text{ GeV}$ and $m_t = 175 \text{ GeV}$ [50], with all widths equal to zero apart from $\Gamma_t \approx 1.58 \text{ GeV}$, adopting its tree-level expression). All neutrinos have been considered massless: i.e., $m_{\nu_e} = m_{\nu_\mu} = m_{\nu_\tau} = 0$. The Branching Ratios (BRs) of the Higgs boson were extracted from ref. [51].

We have analysed the processes (1)–(3) over the mass range $60 \text{ GeV} \lesssim M_\phi \lesssim 140 \text{ GeV}$ and for ep CM energy ranging from 0.5 to 3.0 TeV, with special attention devoted to the case $\sqrt{s}_{ep} = 1.36 \text{ TeV}$, corresponding to the collision of an electron/positron beam from LEP II and a proton beam from LHC [41].

Results

In figs. 3–5 we present the dependence of processes (1)–(3) on the collider CM energy, for a selection of Higgs masses: $M_\phi = 60, 80, 100, 120$ and 140 GeV. Summations over all possible combinations of (anti)flavours have been performed (the top contributions in the final states are included⁸), as well as the integration over the initial $g/q(\bar{q})-$ and $\gamma-$ structure functions. A general feature in figs. 3 and 5 is the rapid increase of all the plots with \sqrt{s}_{ep} , especially for $\sqrt{s}_{ep} \gtrsim 1$ TeV. This is because for \sqrt{s}_{ep} much larger than the final particle masses, phase space effects are quantitatively unimportant. The same effect is less evident in fig. 4, since process (2) is affected by the s –channel structure of the corresponding Feynman diagrams, whereas [part of] these are in t –channel for process [(1)](3). We also notice that the cross section for the process $ep \rightarrow W^\pm \phi X$ is much larger than that of $ep \rightarrow Z^0 \phi X$. This is due to two reasons: first, the coupling $\phi W^+ W^-$ is larger than $\phi Z^0 Z^0$ and second, in process (1) there are additional diagrams (i.e., # 9–12 in fig. 1), some of which (i.e., # 11 and 12) are not suppressed by Yukawa couplings.

In Tab. I we give the cross sections at the LEP \otimes LHC CM energy $\sqrt{s}_{ep} = 1.36$ TeV. To show the importance of the relative contributions of the various flavours entering in the subprocesses (1)–(3), we give their separate rates in Tab. II at $M_\phi = 60$ GeV. For reaction (1) at a fixed \sqrt{s}_{ep} , increasing the Higgs mass reduces the top quark contributions, this is due to the limited phase space available, while the light flavours contributions (i.e., $q = u, d, s, c$ and b) do not change significantly. For example, the top contribution to process (1) diminishes from 1.4% to 0.12% when M_ϕ increases from 60 to 140 GeV, whereas the contributions from *up* (*down*) [*strange*] [*charm*]–initiated processes vary from ≈ 53 (35) [8] {3}% to ≈ 64 (29) [5] {2}%. For process (2) there is no substantial phase space effect of this kind, since we cannot have top contributions here. Thus the numbers do not differ as much: they are ≈ 74 (16) [4] {5} $< 0.6 >$ % to ≈ 80 (14) [3] {3} $< 0.33 >$ %, with the numbers in the “brackets” $<>$ corresponding to b –contributions. For reaction (3), things change dramatically because, on the one hand, top–lines are not connected to the initial state as in (1) and the phase space suppression due to the large top mass is important only if $\sqrt{s}_{ep} \lesssim 1$ TeV, and on the other hand, the Higgs always couples to the very massive top–quark through the ($\sim m_t$) Yukawa coupling, in all Feynman diagrams at tree–level. Because of this $\sim m_q$ coupling the very light flavours $q = u, d$ and s give here completely negligible contributions, while c – and b –fractions are suppressed by a factor of $\approx (m_t/m_c)^2 \approx 10^4$ and $\approx (m_t/m_b)^2 \approx 1225$, with respect to the top ones. Therefore, for process (3), the top–contribution is by far the dominant one for $\sqrt{s}_{ep} \gtrsim 1$ TeV and all ϕ –masses⁹. The corresponding numbers at the LEP \otimes LHC energy, varying M_ϕ in the range 60 – 140 GeV, are: ≈ 0.0016 – 0.0013 % for u –, ≈ 0.0013 – 0.0011 % for d –, ≈ 0.29 – 0.28 % for s –, ≈ 17 – 20 % for c –, ≈ 14 – 21 % for b – and ≈ 69 – 58 % for t –quarks.

Next, we checked if neglecting diagrams 1–6 [and 9–10] of process (2)[(1)] inside the matrix elements, as done in ref. [41], where all quark masses were set equal to zero, could be

⁸As a first approximation only combinations of two flavours within the same quark doublet have been computed for process (1), setting all Cabibbo–Kobayashi–Maskawa terms equal to one.

⁹Whereas for $\sqrt{s}_{ep} \lesssim 1$ TeV the c –contribution is the largest one: in this case the effect of the $q\gamma$ electromagnetic coupling, which favours c –quarks, is dominant on the Yukawa $q\phi$ electroweak one, which favours b –quarks.

a source of error¹⁰. In doing this we needed to apply some cuts to avoid collinear and soft singularities (in the couplings of the incoming photon to the outgoing quark q_{out}) that would otherwise make our amplitudes divergent. To do this, we require, e.g., $|\cos \theta_{\gamma q_{\text{out}}}| < 0.95$ and $|p_{q_{\text{out}}}| > 3$ GeV: restrictions which are reasonably compatible with eventual requirements from the detectors¹¹. Setting again $\sqrt{s}_{ep} = 1.36$ TeV and $M_\phi = 60$ GeV, we have found percentage differences only of the order of 1 in 1000 in the case of light flavour final states, and of $\approx 2\%$ for the contribution $b\gamma \rightarrow tW^-\phi + \text{c.c.}$, in process (1). For reaction (2), differences are appreciable only in the case of c - and b -quarks, these being $\approx 3\%$ and $\approx 13\%$, respectively. These mass effects are approximately the same over the whole intermediate M_ϕ range. However, due to the relative flavour contributions of Tabs. IIa–IIb, when one sums over all of these the effects are largely washed out. We also notice that the errors due to neglecting the quark masses are larger for process (2) than for (1), since in the latter there are also contributions (dominant with respect to the Higgs bremsstrahlung) coming from $\gamma \rightarrow W^+W^-$ splitting whereas at tree-level there is no corresponding $\gamma \rightarrow Z^0Z^0$ coupling. Obviously, taking into account the masses in process (3) is crucial, since there the Higgs is always produced through the Yukawa couplings $q\phi$.

We know that in the mass range $60 \text{ GeV} \lesssim M_\phi \lesssim 140 \text{ GeV}$ the dominant Higgs decay mode is $\phi \rightarrow b\bar{b}$. The corresponding BR in the above interval varies from ≈ 0.85 at $M_\phi = 60$ GeV to ≈ 0.38 at $M_\phi = 140$ GeV, where the off-shell $W^{\pm*}W^\mp$ decay channel begins to be competitive [51]. So, in order to maximise the number of signal events we look for the $\phi \rightarrow b\bar{b}$ signature. We further require flavour identification of b -jets, exploiting the possibilities offered by b -tagging techniques, to reduce the large QCD backgrounds.

In processes (1)–(3) we have additional decaying particles¹²: a W^\pm in $q\gamma \rightarrow q'W^\pm\phi$, a Z^0 in $q\gamma \rightarrow qZ^0\phi$ and two t 's in the $g\gamma \rightarrow t\bar{t}\phi$ contribution. So we expect the following possible final signatures¹³:

$$\begin{aligned} ep \rightarrow W^\pm\phi X &\rightarrow (\ell\nu_\ell)(b\bar{b})X, \\ ep \rightarrow Z^0\phi X &\rightarrow (\ell\bar{\ell})(b\bar{b})X, \end{aligned} \quad (9)$$

or

$$\begin{aligned} ep \rightarrow W^\pm\phi X &\rightarrow (jj)(b\bar{b})X, \\ ep \rightarrow Z^0\phi X &\rightarrow (jj)(b\bar{b})X, \end{aligned} \quad (10)$$

(where X represents the untagged particles in the final states) depending on whether the electroweak massive vector bosons decay leptonically or hadronically, respectively¹⁴. As for

¹⁰We expect differences coming from phase space effects to be negligible for the light flavours u, d, s, c and b , since $m_q \ll \sqrt{s}_{ep}$ for all of them.

¹¹Since similar cuts were not listed in ref. [41], we were unable to reproduce exactly the numbers there computed.

¹²In principle, we also have t -quarks in process (1) which could decay to bW -pairs, but in practise, contributions involving top quarks are here generally quite small if compared to those of the other flavours and substantially negligible when we sum up all different combinations.

¹³We know that in all processes (1)–(3) we can have additional b 's from t/Z^0 -decays or $b\gamma/g\gamma$ -fusion, but we assume that complications coming from the fact of taking in those events a wrong combination $b\bar{b}$ can be largely avoided if we restrict to keep $b\bar{b}$ -invariant masses in the window $|M_{b\bar{b}} - M_\phi| < 5$ GeV (see later on).

¹⁴We do not exploit here possible missing energy decays $Z^0 \rightarrow \nu\bar{\nu}$ in process (2).

process (3) we expect the signature

$$ep \rightarrow q\bar{q}\phi X \rightarrow jj(b\bar{b})X \quad (11)$$

for light quark contributions, and

$$ep \rightarrow t\bar{t}\phi X \rightarrow b\bar{b}W^\pm(b\bar{b})X \quad (12)$$

for top-quarks (with $\text{BR}(t \rightarrow bW) \approx 1$).

Therefore out of the $\approx 56 - 22[6 - 0.6]$ initial femtobarns of reaction (1)[(2)] at $\sqrt{s}_{ep} = 1.36$ TeV and for $M_\phi = 60 - 140$ GeV, assuming $\mathcal{L} = 3 \text{ fb}^{-1}$, we expect $\approx 99 - 18[11 - < 1]$ events for hadronic decays, and $\approx 42 - 8[2 - < 1]$ for leptonic modes, whereas for reaction (3), starting from $\approx 3.8 - 0.24$ fb, we end up with $\approx 10 - < 1$ events (7 of these come from $t\bar{t}\phi$ production with $M_\phi = 60$ GeV), per year.

The irreducible backgrounds to the above signatures are $ep \rightarrow W^\pm Z^0 X \rightarrow W^\pm(b\bar{b})X$ and $ep \rightarrow t\bar{b}X \rightarrow b\bar{b}W^\pm X$ for process (1), $ep \rightarrow Z^0 Z^0 X \rightarrow Z^0(b\bar{b})X$ for (2), and $ep \rightarrow q\bar{q}Z^0 X \rightarrow q\bar{q}(b\bar{b})X$ for (3). These are always present, independently of the W^\pm/Z^0 decay modes in processes (1)–(2). In addition, multi-jet photoproduction, $W^\pm + \text{jets}$, $Z^0 + \text{jets}$ and $t\bar{t}X \rightarrow b\bar{b}W^\pm X$ production and decay events must be also considered.

A few remarks concerning the $t\bar{b}X$ background are needed here. We have mentioned earlier that we take the $e \rightarrow \gamma$ conversion efficiency ϵ (into back-scattered photons) equal to 1, which implies that all the incoming electrons are converted into photons and hence removed from the interaction site. This motivates us to consider γp initiated processes only, and not ep ones. Single-top production proceeds in γp collisions through the partonic subprocesses $q\gamma \rightarrow q'W^{\pm*}\gamma \rightarrow q't\bar{b} + q'\bar{t}b \rightarrow q'b\bar{b}W^\pm$ (i.e., via γW^\pm -fusion) and $g\gamma \rightarrow tbW^\pm \rightarrow b\bar{b}W^+W^-$ (i.e., via $\gamma \rightarrow W^+W^-$ splitting and $g\gamma$ -fusion), whereas in ep collisions it happens via $e^-g \rightarrow \nu_e W^{\pm*}g \rightarrow t\bar{b}\nu_e$. While this latter process has a very large cross section (approximately 1200 fb at $\sqrt{s}_{ep} = 1.36$ TeV), the sum of the first two gives rates generally at the level of one order of magnitude larger than the ones of the signal $qW^\pm\phi \rightarrow qW^\pm(b\bar{b})$, for $m_t = 175$ GeV (see below). Therefore, we would like to stress that it is extremely important that an efficiency ϵ greater than $\approx 90\%$ should be achievable, otherwise a non-negligible fraction $(1 - \epsilon)$ of the single-top background proceeding via $W^\pm g$ -fusion would enter in the experimental sample, inducing a strong suppression of the signal versus background ratio. In fact, the production rate of the $qW^\pm\phi$ signal via bremsstrahlung photons is more than ten times smaller than the one via backscattered γ 's [41].

While b -tagging identification should drastically reduce the backgrounds where b -quarks are not present in the final states, this requirement is not generally enough if they are. In this case, one has to look for invariant masses of the $b\bar{b}$ -pair in a window around M_ϕ , since the most part of the signals lie within this region. In the case of top-resonant backgrounds (i.e., $t\bar{b}X$ and $t\bar{t}X$) we can also exploit the cut, e.g., $|M_{bW \rightarrow bjj} - m_t| > 15$ GeV, which should be very effective in reducing hadronic W^\pm -decays since top-peaks are quite narrow (in fact, $\Gamma_t \approx 1.58$ GeV for $m_t = 175$ GeV). Finally, if the Higgs mass turns out to be close to the Z^0 -mass, the precise absolute normalizations of the processes involving $M_{b\bar{b}}$ resonances are needed.

Assuming good b -tagging performances such that it is possible to drastically eliminate the non- b multi-jet photoproduction, $W^\pm + \text{jets}$ and $Z^0 + \text{jets}$ background events [41], and

that the $M_{b\bar{b}}$ cut is sufficient to suppress the above processes in the case of $\gamma^*/g^* \rightarrow b\bar{b}$ splitting, we end up having to deal only with the backgrounds $ep \rightarrow W^\pm Z^0 X \rightarrow W^\pm(b\bar{b})X$, $ep \rightarrow \bar{t}bX \rightarrow b\bar{b}W^\pm X$, $ep \rightarrow Z^0 Z^0 X \rightarrow Z^0(b\bar{b})X$, $ep \rightarrow t\bar{t}X \rightarrow b\bar{b}W^\pm X$ and $ep \rightarrow q\bar{q}Z^0 X \rightarrow q\bar{q}(b\bar{b})X$. Moreover, we should not forget that an additional drastic rejection factor on the multi-jet background comes from requiring that $M_{jj}/M_{\ell\bar{\nu}_\ell,\ell\bar{\ell}}$ has to reproduce M_{W^\pm} or M_{Z^0} for processes (1)–(2), and that $M_{bW \rightarrow bjj} \approx m_t$ for (3) when $q = t$ (since this flavour is by far the largest partonic contribution at the LEP \otimes LHC energy).

In order to study the background rates, we have implemented their matrix elements in FORTRAN codes generated by MadGraph [52] and HELAS [53]¹⁵. The total cross sections of these processes are displayed in Tab. III, at $\sqrt{s}_{ep} = 1.36$ TeV, for the same γ - and $g/q(\bar{q})$ -structure functions and parameters employed for the signal processes. We notice that backgrounds are in general much larger than the corresponding signals, both for the top-resonant cases (continuum backgrounds) and for the $Z^0 \rightarrow b\bar{b}$ ones (discrete backgrounds). While in the former case this happens because of the top-resonant peaks, in the latter we have that the qZ^0 coupling does not depend on the q -mass (contrary to the Higgs one), so light quarks give large contributions here. This is especially evident in the case of the reaction $ep \rightarrow q\bar{q}Z^0$. The rates for $ep \rightarrow Z^0 Z^0 X$ are of the same order of magnitude as the signal $ep \rightarrow Z^0 \phi X$: in this case the contributions from Z^0 -bremsstrahlung off quarks in the background (we do not have triple vector boson vertices in this case) are comparable to those of the signal in which ϕ is emitted from a Z^0 -line.

However, in principle these very large rates should not be a problem since processes $ep \rightarrow W^\pm Z^0 X$, $ep \rightarrow Z^0 Z^0 X$ and $ep \rightarrow q\bar{q}Z^0 X$ are really important only when $M_\phi \approx M_{Z^0}$, whereas $ep \rightarrow \bar{t}bX \rightarrow b\bar{b}W^\pm X$ and $ep \rightarrow t\bar{t}X \rightarrow b\bar{b}W^\pm X$ are highly reduced when applying a cut in the $b\bar{b}$ -invariant mass (i.e., $M_{b\bar{b}} \approx M_\phi$) and eventually, for W^\pm -hadronic decays, also the cut $M_{bW} \approx m_t$ can be used. In fig. 6 we give the differential distributions in the invariant mass $M_{b\bar{b}}$ for those backgrounds in which the $b\bar{b}$ -pair does not come from a Z^0 -resonance: i.e., $\bar{t}bX \rightarrow b\bar{b}W^\pm X$ and $t\bar{t}X \rightarrow b\bar{b}W^\pm X$ (W^\pm -BRs are not included). For backgrounds containing a $Z^0 \rightarrow b\bar{b}$ resonance, we naively assume that all the $M_{b\bar{b}}$ spectrum is contained in the region $|M_{b\bar{b}} - M_{Z^0}| \leq 2\Gamma_{Z^0} = 5$ GeV.

Since we are concentrating on $b\bar{b}$ -invariant masses in the M_ϕ -region, we require that $M_{b\bar{b}}$ of all events is in the window $|M_{b\bar{b}} - M_\phi| < 5$ GeV, assuming that 10 GeV will be the mass resolution of the detectors. The fractions of the total cross sections from $\bar{t}bX$ - and $t\bar{t}X$ -production which pass this cut are given by the area under the $M_{b\bar{b}}$ distributions of fig. 6 between $M_\phi - 5$ and $M_\phi + 5$ GeV, while we assume that those of the Z^0 -resonant $b\bar{b}$ -events are given by the formula [33]

$$\delta\sigma(Z^0) = \sigma(Z^0) \frac{\max(0, 10 \text{ GeV} - |M_\phi - M_{Z^0}|)}{10 \text{ GeV}}. \quad (13)$$

In using the above equation we tacitly assumed that the $\phi \rightarrow b\bar{b}$ peaks are also all contained in a region of 10 GeV around the ϕ -pole¹⁶. The number of signal (S) and background (B) events and their statistical significance (S/\sqrt{B}) are given in Tab. IV, for the three processes

¹⁵Since process $ep \rightarrow t\bar{t}X \rightarrow b\bar{b}W^\pm X$ was already studied in ref. [54], we also checked that the helicities amplitudes we obtained reproduce the results of that paper (for bremsstrahlung photons).

¹⁶In fact, the Higgs width at $M_\phi = 140$ GeV is $\Gamma_\phi \approx 0.01$ GeV.

(1)–(3) and the sum of their backgrounds separately, for the usual selection of ϕ –masses, after the $M_{b\bar{b}}$ cut. BRs of hadronic and leptonic W^\pm/Z^0 –decays, giving the signatures in eqs. (9)–(12), are included both for processes (1)–(2) and for the backgrounds. We do not make any assumption about the W^\pm –decays when $q = t$ in process (3) and on the second W^\pm in tbX and $t\bar{t}X$, treating them completely inclusively (i.e., such that W^\pm ’s can decay either hadronically or leptonically).

If, as criteria for the observability of a signal, we require a rate $S \geq 6$ events with a significance $S/\sqrt{B} > 4$ for the detection of an isolated Higgs peak, while for the case of Higgs peaks overlapping with Z^0 peaks we require $S \geq 10$ with $S/\sqrt{B} > 6$ [33], then we see from Tab. IV that the situation seems to be discouraging both for hadronic and leptonic W^\pm – and Z^0 –decays, if $M_\phi \gtrsim 80$ GeV. It does not look much better if one tries to make an “inclusive” analysis, summing the rates for signals and backgrounds, as done in Tab. V. This happens because the largest signal (i.e., $W^\pm\phi X$) has a huge background, whereas the other two signals (i.e., $Z^0\phi X$ and $q\bar{q}\phi X$), even though virtually free from backgrounds, give very few events.

Therefore, in the case of overlapping peaks it does not appear to be any possibility to disentangle the signals (see Tabs. I and III), even after a few years of running. However, if $|M_\phi - M_{Z^0}| \gtrsim 5$ GeV, region where only the continuum backgrounds are effective, one can exploit (in the case of hadronic W^\pm –decays) the restriction $|M_{bW \rightarrow bjj} - m_t| > 15$ GeV (for both the combinations bW^+ and $\bar{b}W^+$, assuming to tag the positive gauge boson). For this, in fig. 7 we plot the differential distributions in $M_{b\bar{b}}$ of the $t\bar{b}X$ and $t\bar{t}X$ backgrounds, after applying the above M_{bW} cut. It is clear then how this cut turns out to be extremely useful in rejecting the continuum backgrounds, since their rates are now reduced of $\approx 81\%$ (for $t\bar{b}X$) and of $\approx 97\%$ (for $t\bar{t}X$). If we insert these reduction factors in Tabs. IV–V the scenario changes completely, since we have now to divide all B ’s by a factor of ≈ 13 , and multiply all S/\sqrt{B} ’s by $\approx \sqrt{13}$. This gives significancies much larger than 4 over almost all the intermediate Higgs mass range ($M_\phi \lesssim 120$ GeV). At the same time, the reduction factor for $W^\pm\phi X$ is just a few percent, since the corresponding distribution in M_{bW} is nearly flat (see fig. 8): e.g., approximately 7% for $M_\phi = 60$ GeV and 8% for $M_\phi = 140$ GeV.

A few comments concerning the mass resolution, $|M_\phi - M_{b\bar{b}}| < 5$ GeV, that we have used throughout this paper are worth mentioning at this point. In ref. [38], a larger value was adopted. Here, the fact that we perform the analysis at the parton level would enable us to use for consistency a value of ≈ 7 GeV [18] (which corresponds to a resolution between 11 and 12.3 GeV at the jet–level). In addition, it has to be remembered that the real performances of a possible ep CERN collider are not predictable at the moment, and it is not inconceivable that by the time the LEP \otimes LHC machine comes into operation further progresses in resolving the mass spectra can be achieved. Therefore, for the time being, we deliberately chose a smaller and more optimistic value. However, if eventually it turns out that such a performance will not be feasible, the rates for a worse mass resolution (say 10 GeV) can be readily deduced from the ones given here. In fact, for the signals, due to the small Higgs width in the intermediate mass range, they remain practically unchanged. For the case of the discrete backgrounds we expect smaller significancies only in the region around the Z^0 peak, where it is already impossible to disentangle Higgs signals for a mass resolution of 5 GeV. Finally, for the continuum backgrounds, the numbers would be roughly

a factor two bigger (see figs. 6–7). Therefore, an additional (overall) reduction factor of $\approx \sqrt{2}$ is expected, which should be compensated for by a year of extra running at the same luminosity, with respect to the case of higher mass resolution.

So far we have assumed a 100% acceptance and detection efficiencies for j/ℓ 's in the final states, the same for b -tagging. This is obviously completely unrealistic, and before drawing definite conclusions a full analysis (including kinematical cuts, detector efficiencies, hadronization effects, etc ...) should be done. We adopt here the set of kinematical cuts given in ref. [38]. As the substantial part of Higgs signals would come from reaction (1), which furthermore is the most affected by competitive backgrounds (contrary to processes (2)–(3), which are virtually free from backgrounds in the region where Higgs signals can be disentangled, $M_\phi \neq M_{Z^0}$), we perform the study for the case $W^\pm \phi X$ and for the corresponding (continuum) backgrounds.

If we assume as acceptance region the one defined by¹⁷:

- transverse momentum p_T^i of at least 20 GeV;
- pseudorapidity $|\eta_i|$ less than 4.5;
- separation $\Delta R_{ij} = \sqrt{\Delta\eta_{ij} + \Delta\varphi_{ij}} > 1$;

for all the i -th and j -th b 's and jets of the signature $b\bar{b}jjX$, then the reduction factors for the $W^\pm \phi X$ signal and the $t\bar{b}X$ and $t\bar{t}X$ background rates are: $R \approx 16 - 7$ (for $M_\phi = 60 - 140$ GeV), ≈ 14 and ≈ 11 , respectively.

That means that, on the one hand, the number of events is reduced to a few units per year (from ≈ 3 at $M_\phi = 140$ GeV to ≈ 8 at $M_\phi = 60$ GeV, for hadronic W^\pm -decays) whereas, on the other hand, the effect on the significancies is a reduction factor approximately equal to 4(2), for $M_\phi = 60(140)$ GeV. Therefore, we would conclude that even though these selection criteria act in the direction of favouring the backgrounds, largely spoiling the effectiveness of the $M_{bW \rightarrow bjj}$ cut, nevertheless, the final values we obtain for S , B and S/\sqrt{B} shouldn't substantially modify our above positive conclusions, but only imposing the requirement of accumulating a higher luminosity (in at least two years time), in order to clearly disentangle Higgs signals. In general, we would like to stress here that our choice of kinematical cuts could well be different from the one which will be at the end imposed by the real LEP \otimes LHC detectors. At present, in fact, the acceptances of these latter have yet not been looked into, as even the most recent and complete studies on the argument only deal with simulations done for the LHC (see the ATLAS [55] and CMS [56] Technical Proposals). That is, we wonder if detectors designed for a pp machine will be the same and/or will work in the same configuration even when they will be set up around a different kind of machine, an ep collider. Nothing prevent us then from thinking that by the time the LEP \otimes LHC collider will be operating both the improvement in the detection techniques and the necessity to design the detectors in view of their best performances at an ep machine, could end up by reducing the impact of the acceptance cuts on the event selection procedure.

Concerning flavour identification, it is clear that high b -tagging performances and excellent not- b rejection are needed, at least as the ones expected at the LHC in the pp mode [18].

¹⁷In the case of the signal no requirement is imposed on the spectator jet from the q' -quark in (1).

Before concluding, we notice here how processes like (1)–(3) could turn out to be extremely interesting if one considers their counterparts, e.g., in the Minimal Supersymmetric Standard Model (\mathcal{MSSM}). Here quark–Higgs couplings proportional to $\tan\beta$ can enhance the signals up to $\mathcal{O}(1000)$ times for very large $\tan\beta$. This drastic enhancement happens when considering the contribution of diagrams involving the bremsstrahlung of the pseudoscalar boson A^0 off massive *down*–type quarks (i.e., b –quarks: hence masses should be included). This occurs in all the Feynman diagrams of process (3), while it only happens for the suppressed graphs 1–6 [and 9,10] in (2)[(1)]. These latter contribute to the total rate at the level of % for the \mathcal{SM} case but are the only surviving ones for the \mathcal{MSSM} (since the pseudoscalar boson A^0 does not couple to vector bosons at tree–level). In addition, in processes (1)–(3), once we substitute ϕ by one of the \mathcal{MSSM} neutral Higgses H^0 , h^0 and A^0 and we also include the flavour changing cases in which $\phi \leftrightarrow H^\pm$ and double Higgs productions in $q\gamma$ fusion ($W^\pm \leftrightarrow H^\pm$ and $Z^0 \leftrightarrow H^0, h^0, A^0$), we will have a very rich laboratory where all the fundamental interactions of the \mathcal{MSSM} can be carefully studied. A complete analysis within this Model will be presented elsewhere [57].

Summary and conclusions

In summary, we have studied the production cross sections of the \mathcal{SM} Higgs ϕ with mass in the range $60 \text{ GeV} \lesssim M_\phi \lesssim 140 \text{ GeV}$ at a next–generation ep collider, with $500 \text{ GeV} \lesssim \sqrt{s}_{ep} \lesssim 3 \text{ TeV}$, through the partonic processes

$$\gamma q(\bar{q}) \rightarrow q'(\bar{q}') W^\pm \phi,$$

$$\gamma q(\bar{q}) \rightarrow q(\bar{q}) Z^0 \phi$$

and

$$g\gamma \rightarrow q\bar{q}\phi,$$

for all possible (massive) flavours of the quarks $q(q')$, with incoming photons generated via Compton back–scattering of laser light.

Special attention has been devoted to the case of the planned CERN LEP \otimes LHC ep collider (with $\sqrt{s}_{ep} \approx 1.36 \text{ TeV}$), where signatures in which the Higgs decays to $b\bar{b}$ –pairs were studied, exploiting the possibilities given by b –tagging techniques.

We concluded that at this machine, apart from the case $M_\phi \approx M_{Z^0}$ which is impossible to disentangle, Higgs signals should be detectable above all the possible backgrounds over the most part of the remaining intermediate mass range, by searching for the hadronic decays of W^\pm ’s in process (1), in particular after approximately a couple of years running at the luminosity $\mathcal{L} = 3 \text{ fb}^{-1}$ if $M_\phi \lesssim 120 \text{ GeV}$. Due to the fact that the leptonic decay channels of the W^\pm ’s give small rates and that a cut in the invariant mass M_{bW} is not applicable in this case, no possibility of detections exists if $W^\pm \rightarrow \ell\bar{\nu}_\ell$. Therefore, in this respect, we disagree with the conclusions given in ref. [41]. In the case of processes (2)–(3), after the acceptance cuts here adopted we expect to get significant number of events only for a value of \mathcal{L} much bigger than the one assumed here (more than an order of magnitude).

In general, if the LHC detectors will not be able to achieve the necessary performances for all the foreseen Higgs measurements, then the LEP \otimes LHC collider option could provide

interesting prospects of studying the \mathcal{SM} Higgs boson parameters (i.e., M_ϕ , Γ_ϕ , BRs, etc ...) in the intermediate mass range, in an environment partially free from the QCD background typical of $pp/p\bar{p}$ accelerators, especially if larger b -tagging performances and/or a high luminosity can be achieved, in advance of a possible future NLC.

Acknowledgments

We are grateful to J.B. Tausk for interesting discussions and useful suggestions, to T. Stelzer for his helpful advice on using MadGraph and to W.J. Stirling for reading the manuscript.

Appendix

In this section we present the explicit formulae for the helicity amplitudes of the processes we have studied. Definitions of S , Y and Z functions and of other quantities (p , λ , μ , η , etc...), which enter in the following, can be found in ref. [58], with identical notation.

Here, we introduce the definitions:

$$-b_1 = -b_2 = b_3 = 2b_4 = 2b_5 = 2b_6 = 2b_7 = 1 \quad (14)$$

for the coefficients of the incoming/outgoing four-momenta,

$$D_V(p) = \frac{1}{p^2 - M_V^2}, \quad D_q(p) = \frac{1}{p^2 - m_q^2} \quad (15)$$

for the propagators, where $V = W^\pm, Z^0$ and $q = u$ or d ,

$$N_i = [4(p_i \cdot q_i)]^{-1/2}, \quad i = 1, 2 \quad (16)$$

for the gluon ($i = 1$) and photon ($i = 2$) normalisation factor, where $p_i(q_i)$ is the massless vector four-momentum (any four-vector not proportional to p_i), with $i = 1, 2$ [43]. The symbols r_1 and r_2 represent two light-like four-momenta satisfying the relations

$$r_1^2 = r_2^2 = 0, \quad r_1^\mu + r_2^\mu = p_4^\mu, \quad (17)$$

($d\Omega_{r_1(r_2)}$ indicates the solid angle of $r_{1(2)}$ in the rest frame of p_4) [43], p_6 and p_7 are antispinor four-momenta such that

$$p_6^\mu \equiv p_4^\mu, \quad p_7^\mu \equiv p_5^\mu, \quad (18)$$

and

$$\sum_{\lambda=\pm} u(p_i, \lambda) \bar{u}(p_i, \lambda) = \not{p}_i - m_i, \quad \text{with } i = 6, 7, \quad (19)$$

while

$$\sum_{\lambda=\pm} u(p_i, \lambda) \bar{u}(p_i, \lambda) = \not{p}_i + m_i, \quad \text{with } i = 4, 5. \quad (20)$$

We also define the spinor functions¹⁸

$$\mathcal{X}_2 = \sum_{\lambda=\pm} \sum_{i=1,3} (-b_i) Y([2]; [i]; 1, 1) Y([i]; (2); 1, 1),$$

¹⁸Throughout this appendix we adopt the symbol $\{\lambda\}$ to denote a set of helicities of all external particles in a given reaction, $\sum_{\{\lambda\}}$ to indicate the usual sum over all their possible combinations, and the symbol $\sum_{i=j,k,l,\dots}$ to indicate a sum over j, k, l, \dots with index i .

$$\begin{aligned}
\mathcal{X}_4 &= \sum_{\lambda=\pm} \sum_{i=5,7} b_i Y(\{1\}; [i]; 1, 1) Y([i]; \{2\}; 1, 1), \\
\mathcal{X}_{31}^{qV(\prime)} &= \sum_{\lambda=\pm} \sum_{i=4,6(5,7)} b_i Y([3]; [i]; 1, 1) Y([i]; [1]; c_{R_V}^q, c_{L_V}^q), \\
\mathcal{Y}_2^{(\prime)} &= \sum_{\lambda=\pm} \sum_{i=4,6(5,7)} b_i Y([2]; [i]; 1, 1) Y([i]; (2); 1, 1), \\
\mathcal{Y}_4 &= \sum_{\lambda=\pm} Y(\{1\}; p_2, \lambda; 1, 1) Y(p_2, \lambda; \{2\}; 1, 1), \\
\mathcal{F}_{31}^{qV} &= \mu_1 \eta_1 Y([3]; [1]; c_{L_V}^q, c_{R_V}^q) - \mu_3 \eta_3 Y([3]; [1]; c_{R_V}^q, c_{L_V}^q), \\
\mathcal{Y}_{31}^{qV} &= \sum_{\lambda=\pm} Y([3]; p_2, \lambda; 1, 1) Y(p_2, \lambda; [1]; c_{R_V}^q, c_{L_V}^q), \\
\tilde{\mathcal{Y}}_{31}^{qV} &= \mathcal{Y}_{31}^{qV} - \frac{\mathcal{F}_{31}^{qV}}{M_V^2} p_2 \cdot (p_4 + p_5), \\
\mathcal{Z}_{24} &= Z([2]; (2); \{1\}; \{2\}; 1, 1; 1, 1), \\
\mathcal{Z}_{312}^{qV} &= Z([3]; [1]; [2]; (2); c_{R_V}^q, c_{L_V}^q; 1, 1), \\
\tilde{\mathcal{Z}}_{312}^{qV} &= \mathcal{Z}_{312}^{qV} - \frac{\mathcal{F}_{31}^{qV}}{M_V^2} (\mathcal{Y}_2 + \mathcal{Y}'_2), \\
\mathcal{Z}_{314}^{qV} &= Z([3]; [1]; \{1\}; \{2\}; c_{R_V}^q, c_{L_V}^q; 1, 1), \\
\tilde{\mathcal{Z}}_{314}^{qV} &= \mathcal{Z}_{314}^{qV} - \frac{\mathcal{F}_{31}^{qV}}{M_V^2} (\mathcal{X}_4 - \mathcal{Y}_4), \tag{21}
\end{aligned}$$

where V represents a gauge boson W^\pm , Z^0 or γ , $q = u$ or d (u - and d -type quarks of arbitrary masses m_u and m_d , respectively), and with the short-hand notations $[x] = p_x, \lambda_x$ ($x = 1, \dots, 4$), $(x) = q_x, \lambda_x$ ($x = 1, 2$) and $\{x\} = r_x, -$ ($x = 1, 2$).

In the following we adopt $[i] = p_i, \lambda$ and $[j] = p_j, \lambda'$, whereas the couplings c_R , c_L and \mathcal{H} can be easily deduced from tabs. VI–VII. Also, we sometimes make use of the equalities

$$\mathcal{Y}_2 + \mathcal{Y}'_2 = \mathcal{X}_2, \quad \mathcal{X}_{31}^{qV} + \mathcal{X}_{31}^{qV'} = \mathcal{Y}_{31}^{qV} + \mathcal{F}_{31}^{qV}. \tag{22}$$

1. Process $d\gamma \rightarrow uW^-\phi$.

In order to obtain from fig. 1 the Feynman graphs of the process

$$d(p_1, \lambda_1) + \gamma(p_2, \lambda_2) \longrightarrow u(p_3, \lambda_3) + W^-(p_4) + \phi(p_5), \tag{23}$$

one has to make the following assignments:

$$q = d, \quad q' = u, \quad V^{(*)} = W^{\pm(*)}. \tag{24}$$

The corresponding matrix element, summed over final spins and averaged over initial ones, is given by

$$|\overline{M}| = \frac{e^6}{4} N_2^2 \frac{3}{8\pi M_{W^\pm}^2} \sum_{\{\lambda\}} \int d\Omega_{r_1(r_2)} \sum_{l,m=1}^{12} T_l^{\{\lambda\}} T_m^{\{\lambda\}*}, \quad (25)$$

where

$$\begin{aligned} iT_1^{\{\lambda\}} &= D_u(p_3 + p_5) D_d(p_1 + p_2) M_1^{\{\lambda\}} \mathcal{H}_1, & iT_2^{\{\lambda\}} &= D_d(p_3 + p_4) D_d(p_1 + p_2) M_2^{\{\lambda\}} \mathcal{H}_2, \\ iT_3^{\{\lambda\}} &= D_d(p_3 + p_4) D_d(p_1 - p_5) M_3^{\{\lambda\}} \mathcal{H}_3, & iT_4^{\{\lambda\}} &= D_u(p_3 + p_5) D_u(p_1 - p_4) M_4^{\{\lambda\}} \mathcal{H}_4, \\ iT_5^{\{\lambda\}} &= D_u(p_3 - p_2) D_u(p_1 - p_4) M_5^{\{\lambda\}} \mathcal{H}_5, & iT_6^{\{\lambda\}} &= D_u(p_3 - p_2) D_d(p_1 - p_5) M_6^{\{\lambda\}} \mathcal{H}_6, \\ iT_7^{\{\lambda\}} &= D_{W^\pm}(p_4 + p_5) D_d(p_1 + p_2) M_7^{\{\lambda\}} \mathcal{H}_7, & iT_8^{\{\lambda\}} &= D_{W^\pm}(p_4 + p_5) D_u(p_3 - p_2) M_8^{\{\lambda\}} \mathcal{H}_8, \\ iT_9^{\{\lambda\}} &= D_{W^\pm}(p_2 - p_4) D_u(p_3 + p_5) M_9^{\{\lambda\}} \mathcal{H}_9, & iT_{10}^{\{\lambda\}} &= D_{W^\pm}(p_2 - p_4) D_d(p_1 - p_5) M_{10}^{\{\lambda\}} \mathcal{H}_{10}, \\ iT_{11}^{\{\lambda\}} &= D_{W^\pm}(p_1 - p_3) D_{W^\pm}(p_4 + p_5) M_{11}^{\{\lambda\}} \mathcal{H}_{11}, & iT_{12}^{\{\lambda\}} &= D_{W^\pm}(p_1 - p_3) D_{W^\pm}(p_2 - p_4) M_{12}^{\{\lambda\}} \mathcal{H}_{12}. \end{aligned} \quad (26)$$

We have

$$\begin{aligned} M_1^{\{\lambda\}} &= \sum_{\lambda=\pm} \sum_{\lambda'=\pm} \sum_{i=3,5,7} \sum_{j=1,2} (-b_i b_j) Y([3]; [i]; c_{R_\phi}^u, c_{L_\phi}^u) \\ &\quad \times Z([i]; [j]; \{1\}; \{2\}; c_{R_{W^\pm}}, c_{L_{W^\pm}}; 1, 1) Z([j]; [1]; [2]; (2); c_{R_\gamma}^d, c_{L_\gamma}^d; 1, 1), \\ M_2^{\{\lambda\}} &= \sum_{\lambda=\pm} \sum_{\lambda'=\pm} \sum_{i=3,4,6} \sum_{j=1,2} (-b_i b_j) Z([3]; [i]; \{1\}; \{2\}; c_{R_{W^\pm}}, c_{L_{W^\pm}}; 1, 1) \\ &\quad \times Y([i]; [j]; c_{R_\phi}^d, c_{L_\phi}^d) Z([j]; [1]; [2]; (2); c_{R_\gamma}^d, c_{L_\gamma}^d; 1, 1), \\ M_3^{\{\lambda\}} &= \sum_{\lambda=\pm} \sum_{\lambda'=\pm} \sum_{i=3,4,6} \sum_{j=1,5} (-b_i b_j) Z([3]; [i]; \{1\}; \{2\}; c_{R_{W^\pm}}, c_{L_{W^\pm}}; 1, 1) \\ &\quad \times Z([i]; [j]; [2]; (2); c_{R_\gamma}^d, c_{L_\gamma}^d; 1, 1) Y([j]; [1]; c_{R_\phi}^d, c_{L_\phi}^d), \\ M_4^{\{\lambda\}} &= \sum_{\lambda=\pm} \sum_{\lambda'=\pm} \sum_{i=3,5,7} \sum_{j=1,4,6} (-b_i b_j) Y([3]; [i]; c_{R_\phi}^u, c_{L_\phi}^u) \\ &\quad \times Z([i]; [j]; [2]; (2); c_{R_\gamma}^u, c_{L_\gamma}^u; 1, 1) Z([j]; [1]; \{1\}; \{2\}; c_{R_{W^\pm}}, c_{L_{W^\pm}}; 1, 1), \\ M_5^{\{\lambda\}} &= \sum_{\lambda=\pm} \sum_{\lambda'=\pm} \sum_{i=3,2} \sum_{j=1,4,6} (-b_i b_j) Z([3]; [i]; [2]; (2); c_{R_\gamma}^u, c_{L_\gamma}^u; 1, 1) \\ &\quad \times Y([i]; [j]; c_{R_\phi}^u, c_{L_\phi}^u) Z([j]; [1]; \{1\}; \{2\}; c_{R_{W^\pm}}, c_{L_{W^\pm}}; 1, 1), \\ M_6^{\{\lambda\}} &= \sum_{\lambda=\pm} \sum_{\lambda'=\pm} \sum_{i=3,2} \sum_{j=1,5,7} (-b_i b_j) Z([3]; [i]; [2]; (2); c_{R_\gamma}^u, c_{L_\gamma}^u; 1, 1) \\ &\quad \times Z([i]; [j]; \{1\}; \{2\}; c_{R_{W^\pm}}, c_{L_{W^\pm}}; 1, 1) Y([j]; [1]; c_{R_\phi}^d, c_{L_\phi}^d), \\ M_7^{\{\lambda\}} &= \sum_{\lambda=\pm} \sum_{i=1,2} (-b_i) Z([i]; [1]; [2]; (2); c_{R_\gamma}^d, c_{L_\gamma}^d; 1, 1) \\ &\quad \times \{Z([3]; [i]; \{1\}; \{2\}; c_{R_{W^\pm}}, c_{L_{W^\pm}}; 1, 1) \end{aligned}$$

$$\begin{aligned}
& -\frac{\mathcal{X}_4}{M_{W^\pm}^2} \left[\sum_{\lambda'=\pm} \sum_{j=1,2,3} (-b_j) Y([3]; [j]; 1, 1) Y([j]; [i]; c_{R_{W^\pm}}, c_{L_{W^\pm}}) \right] \}, \\
M_8^{\{\lambda\}} &= \sum_{\lambda=\pm} \sum_{i=2,3} (b_i) Z([3]; [i]; [2]; (2); c_{R_\gamma}^u, c_{L_\gamma}^u; 1, 1) \\
&\quad \times \{ Z([i]; [1]; \{1\}; \{2\}; c_{R_{W^\pm}}, c_{L_{W^\pm}}; 1, 1) \\
&\quad - \frac{\mathcal{X}_4}{M_{W^\pm}^2} \left[\sum_{\lambda'=\pm} \sum_{j=1,2,3} (-b_j) Y([i]; [j]; 1, 1) Y([j]; [1]; c_{R_{W^\pm}}, c_{L_{W^\pm}}) \right] \}, \\
M_9^{\{\lambda\}} &= \sum_{\lambda=\pm} \sum_{i=3,5,7} (2b_i) Y([3]; [i]; c_{R_\phi}^u, c_{L_\phi}^u) \\
&\quad \times \left[\mathcal{Z}_{24} \sum_{\lambda'=\pm} Y([i]; p_2, \lambda'; 1, 1) Y(p_2, \lambda'; [1]; c_{R_{W^\pm}}, c_{L_{W^\pm}}) \right. \\
&\quad \left. - \mathcal{Y}_2 Z(\{1\}; \{2\}; [i]; [1]; 1, 1; c_{R_{W^\pm}}, c_{L_{W^\pm}}) - \mathcal{Y}_4 Z([2]; (2); [i]; [1]; 1, 1; c_{R_{W^\pm}}, c_{L_{W^\pm}}) \right], \\
M_{10}^{\{\lambda\}} &= \sum_{\lambda=\pm} \sum_{i=1,5,7} (-2b_i) Y([i]; [1]; c_{R_\phi}^d, c_{L_\phi}^d) \\
&\quad \times \left[\mathcal{Z}_{24} \sum_{\lambda'=\pm} Y([3]; p_2, \lambda'; 1, 1) Y(p_2, \lambda'; [i]; c_{R_{W^\pm}}, c_{L_{W^\pm}}) \right. \\
&\quad \left. - \mathcal{Y}_2 Z(\{1\}; \{2\}; [3]; [i]; 1, 1; c_{R_{W^\pm}}, c_{L_{W^\pm}}) - \mathcal{Y}_4 Z([2]; (2); [3]; [i]; 1, 1; c_{R_{W^\pm}}, c_{L_{W^\pm}}) \right], \\
M_{11}^{\{\lambda\}} &= \mathcal{Z}_{24} (\mathcal{F}_{31}^{W^\pm} + 2\mathcal{Y}_{31}^{W^\pm}) - 2\mathcal{X}_2 \tilde{\mathcal{Z}}_{314}^{W^\pm} - (2\mathcal{Y}_4 - \mathcal{X}_4) \tilde{\mathcal{Z}}_{312}^{W^\pm} \\
&\quad - \frac{1}{M_{W^\pm}^2} [\mathcal{X}_2 \mathcal{X}_4 (\mathcal{Y}_{31}^{W^\pm} - \mathcal{X}_{31}^{W^\pm} - \mathcal{X}_{31}^{W^\pm'}) + (p_1 - p_3)^2 (\mathcal{Z}_{24} \mathcal{F}_{31}^{W^\pm} + \tilde{\mathcal{Z}}_{312}^{W^\pm} \mathcal{X}_4) + 2p_2 \cdot (p_1 - p_3) \mathcal{Z}_{24} \mathcal{F}_{31}^{W^\pm}] \\
&\quad - \frac{1}{M_{W^\pm}^4} \{ [(p_1 - p_3)^2 + p_2 \cdot (p_1 - p_3)] \mathcal{X}_4 (\mathcal{Y}_2 - \mathcal{Y}'_2) \mathcal{F}_{31}^{W^\pm} \}, \\
M_{12}^{\{\lambda\}} &= 2(\tilde{\mathcal{Y}}_{31}^{W^\pm} \mathcal{Z}_{24} - \mathcal{Y}_2 \tilde{\mathcal{Z}}_{314}^{W^\pm} - \mathcal{Y}_4 \tilde{\mathcal{Z}}_{312}^{W^\pm}). \tag{27}
\end{aligned}$$

2. Process $d\gamma \rightarrow dZ^0\phi$.

The Feynman graphs for the process

$$d(p_1, \lambda_1) + \gamma(p_2, \lambda_2) \longrightarrow d(p_3, \lambda_3) + Z^0(p_4) + \phi(p_5), \tag{28}$$

can be obtained from fig. 1 by setting

$$q = q' = d, \quad V^{(*)} = Z^{0(*)}. \tag{29}$$

The formulae for the amplitude squared are practically the same as in the previous section, considering the first 8 amplitudes only (i.e., $M_i^{\{\lambda\}} = 0$ for $i = 9, \dots, 12$), with the relabeling:

$$u \rightarrow d, \quad W^\pm \rightarrow Z^0, \tag{30}$$

in eqs. (25)–(27).

3. Process $g\gamma \rightarrow u\bar{u}\phi$.

The Feynman diagrams for

$$g(p_1, \lambda_1) + \gamma(p_2, \lambda_2) \longrightarrow u(p_3, \lambda_3) + \bar{u}(p_4, \lambda_4) + \phi(p_5), \quad (31)$$

are shown in fig. 2, where $q = u$. The amplitude squared is

$$|\overline{M}| = \frac{e^4 g_s^2}{4} N_1^2 N_2^2 \sum_{\{\lambda\}} \sum_{l,m=1}^6 T_l^{\{\lambda\}} T_m^{\{\lambda\}*}. \quad (32)$$

The expressions for the $T_i^{\{\lambda\}}$'s are

$$\begin{aligned} -i T_1^{\{\lambda\}} &= D_u(p_3 + p_5) D_u(p_1 - p_4) M_1^{\{\lambda\}} \mathcal{H}_1, & -i T_2^{\{\lambda\}} &= D_u(p_3 - p_2) D_u(p_1 - p_4) M_2^{\{\lambda\}} \mathcal{H}_2, \\ -i T_3^{\{\lambda\}} &= D_u(p_3 - p_2) D_u(p_4 + p_5) M_3^{\{\lambda\}} \mathcal{H}_3, \\ -i T_{i+3}^{\{\lambda\}} &= -i T_i^{\{\lambda\}} (p_3 \leftrightarrow p_4), & i &= 1, \dots, 3, \end{aligned} \quad (33)$$

while the spinor functions are

$$\begin{aligned} M_1^{\{\lambda\}} &= \sum_{\lambda=\pm} \sum_{\lambda'=\pm} \sum_{i=3,5,7} \sum_{j=1,4} (-b_i b_j) Y([3]; [i]; c_{R_\phi}^u, c_{L_\phi}^u) \\ &\quad \times Z([i]; [j]; [2]; (2); c_{R_\gamma}^u, c_{L_\gamma}^u; 1, 1) Z([j]; [4]; [1]; (1); c_{R_g}^u, c_{L_g}^u; 1, 1), \\ M_2^{\{\lambda\}} &= \sum_{\lambda=\pm} \sum_{\lambda'=\pm} \sum_{i=2,3} \sum_{j=1,4} (-b_i b_j) Z([3]; [i]; [2]; (2); c_{R_\gamma}^u, c_{L_\gamma}^u; 1, 1) \\ &\quad \times Y([i]; [j]; c_{R_\phi}^u, c_{L_\phi}^u) Z([j]; [4]; [1]; (1); c_{R_g}^u, c_{L_g}^u; 1, 1), \\ M_3^{\{\lambda\}} &= \sum_{\lambda=\pm} \sum_{\lambda'=\pm} \sum_{i=2,3} \sum_{j=4,5,7} (-b_i b_j) Z([3]; [i]; [2]; (2); c_{R_\gamma}^u, c_{L_\gamma}^u; 1, 1) \\ &\quad \times Z([i]; [j]; [1]; (1); c_{R_g}^u, c_{L_g}^u; 1, 1) Y([j]; [4]; c_{R_\phi}^u, c_{L_\phi}^u), \\ M_{i+3}^{\{\lambda\}} &= M_i^{\{\lambda\}} (p_3 \leftrightarrow p_4), & i &= 1, \dots, 3. \end{aligned} \quad (34)$$

By trivial relabeling and sign exchanges, it is possible to obtain from the above formulae the corresponding ones for the u -type quark initiated processes

$$\begin{aligned} u\gamma &\rightarrow dW^+\phi, \\ u\gamma &\rightarrow uZ^0\phi, \end{aligned} \quad (35)$$

as for the charge conjugate reactions

$$\begin{aligned} \bar{d}\gamma &\rightarrow \bar{u}W^+\phi, \\ \bar{d}\gamma &\rightarrow \bar{d}Z^0\phi. \end{aligned} \quad (36)$$

Finally, the same it can be done for obtaining the helicity amplitudes for the g -initiated process

$$g\gamma \rightarrow d\bar{d}\phi. \quad (37)$$

References

- [1] S.L. Glashow, *Nucl. Phys.* **22** (1961) 579;
S. Weinberg, *Phys. Rev. Lett.* **19** (1967) 1264;
A. Salam, Proceedings of the “*Nobel Symposium*”, ed. N. Svartholm, Almqvist and Wiksell, Stockholm, 1968, 367.
- [2] P.W. Higgs, *Phys. Rev. Lett.* **12** (1964) 132.
- [3] ALEPH Collaboration, *Phys. Rep.* **216** (1992) 253;
DELPHI Collaboration, *Nucl. Phys.* **B373** (1992) 3;
L3 Collaboration, *Phys. Lett.* **B303** (1993) 391;
OPAL Collaboration, *Phys. Lett.* **B253** (1991) 511.
- [4] M. Veltman, *Phys. Lett.* **B70** (1977) 253.
- [5] B.W. Lee, C. Quigg and G.B. Thacker, *Phys. Rev. Lett.* **38** (1977) 883; *Phys. Rev.* **D16** (1977) 1519.
- [6] Proceedings of the “*ECFA Workshop on LEP 200*”,
A. Bohm and W. Hoogland eds., Aachen FRG, 29 Sept.–1 Oct. 1986, CERN 87-08.
- [7] Proceedings of the “*Large Hadron Collider Workshop*”, Aachen, 4–9 October 1990, eds.
G. Jarlskog and D. Rein, Report CERN 90–10, ECFA 90–133, Geneva, 1990.
- [8] J.D. Bjorken, Proceedings of the “*Summer Institute on Particle Physics*”, *SLAC Report* 198 (1976);
B.W. Lee, C. Quigg and H.B. Thacker, *Phys. Rev.* **D16** (1977) 1519;
J. Ellis, M.K. Gaillard and D.V. Nanopoulos, *Nucl. Phys.* **B106** (1976) 292;
B.L. Ioffe and V.A. Khoze, *Sov. J. Part. Nucl.* **9** (1978) 50.
- [9] H. Georgi, S.L. Glashow, M.E. Macahek and D.V. Nanopoulos, *Phys. Rev. Lett.* **40** (1978) 692.
- [10] R.N. Cahn and S. Dawson, *Phys. Lett.* **B136** (1984) 196.
- [11] S.L. Glashow, D.V. Nanopoulos and A. Yildiz, *Phys. Rev.* **D18** (1978) 1724.
- [12] R. Kleiss, Z. Kunszt and W.J. Stirling, *Phys. Lett.*
B253 (1991) 269;
M.L. Mangano, SDC Collaboration note SSC–SDC–90–00113.
- [13] R. Raitio and W.W. Wada, *Phys. Rev.* **D19** (1979) 941;
J.N. Ng and P. Zakarauskas, *Phys. Rev.* **D29** (1984) 876.
- [14] J.F. Gunion, *Phys. Lett.* **B261** (1991) 510;
W.J. Marciano and F.E. Paige, *Phys. Rev. Lett.* **66** (1991) 2433;
A. Ballestrero and E. Maina, *Phys. Lett.* **B268** (1992) 437;
Z. Kunzst, Z. Trócsányi and W.J. Stirling, *Phys. Lett.* **B271** (1991) 247;
D.J. Summers, *Phys. Lett.* **B277** (1992) 366.

- [15] C. Seez et al., in ref.[7].
- [16] J. Dai, J.F. Gunion and R. Vega, *Phys. Rev. Lett.* **71** (1993) 2699.
- [17] *Solenoidal Detector Collaboration Technical Design Report*, E.L. Berger et al., *Report SDC-92-201, SSCL-SR-1215*, 1992.
- [18] D. Froidevaux and E. Richter-Was, *preprint CERN-TH.7459/94*.
- [19] J.F. Gunion, H.E. Haber, G.L. Kane and S. Dawson, “*The Higgs Hunter Guide*” (Addison-Wesley, Reading MA, 1990).
- [20] Proceedings of the Workshop “*Physics and Experiments with Linear Colliders*”, Saariselkä, Finland, 9–14 September 1991, eds. R. Orawa, P. Eerola and M. Nordberg, World Scientific Publishing, Singapore, 1992.
- [21] Proceedings of the Workshop “*e⁺e⁻ Collisions at 500 GeV. The Physics Potential*”, Munich, Annecy, Hamburg, 3–4 February 1991, ed. P.M. Zerwas, DESY pub. 92-123A/B/C, August 1992.
- [22] Proceedings of the ECFA workshop on “*e⁺e⁻ Linear Colliders LC92*”, R. Settles ed., Garmisch Partenkirchen, 25 July–2 Aug. 1992, MPI-PhE/93-14, ECFA 93-154.
- [23] Proceedings of the “*I Workshop on Japan Linear Collider (JLC)*”, KEK 1989, KEK-Report 90-2;
Proceedings of the “*II Workshop on Japan Linear Collider (JLC)*”, KEK 1990, KEK-Report 91-10.
- [24] V. Barger, K. Cheung, A. Djouadi, B.A. Kniehl and P.M. Zerwas, *Phys. Rev.* **D49** (1994) 79.
- [25] D.R.T. Jones and S.T. Petkov, *Phys. Lett.* **B84** (1979) 440;
R.N. Cahn and S. Dawson, *Phys. Lett.* **B136** (1984) 196;
K. Hikasa, *Phys. Lett.* **B164** (1985) 341;
G. Altarelli, B. Mele and F. Pitolli, *Nucl. Phys.* **B287** (1987) 205;
B. Kniehl, *preprint DESY 91-128*, 1991.
- [26] V. Barger, K. Cheung, B.A. Kniehl and R.J. Phillips, *Phys. Rev.* **D46** (1992) 3725.
- [27] K. Hagiwara, J. Kanzaki and H. Murayama, *Durham Univ. Report No. DTP-91-18*, 1991.
- [28] J.F. Gunion and H.E. Haber, *preprint UCD-90-25*, September 1990, Presented at “*1990 DPF Summer Study on High Energy Physics*”, Snowmass, Colorado, June 25–July 13, 1990;
J.F. Gunion and H.E. Haber, in Proceedings of the “*1990 Summer Study on High Energy Physics: Research Directions for the Decade*”, ed. E.L. Berger, Snowmass, Colorado, 1990;
J.F. Gunion and H.E. Haber, *Phys. Rev.* **D48** (1993) 5109.

[29] D. Borden, D. Bauer and D. Caldwell, *SLAC Report No.* SLAC-PUB-5715, 1992;
 F. Richard, in ref. [21];
 D. Bowser-Chao and K. Cheung, *Phys. Rev.* **D48** (1993) 89.

[30] K. Cheung, *Phys. Rev.* **D47** (1993) 3750;
 E. Boos, I. Ginzburg, K. Melnikov, T. Sack and S. Shichanin, *Z. Phys.* **C56** (1992) 487.

[31] E. Boos, M. Dubinin, V. Ilyin, A. Pukhov, G. Jikia and S. Sultanov, *Phys. Lett.* **B273** (1991) 173.

[32] K. Hagiwara, I. Watanabe and P.M. Zerwas, *Phys. Lett.* **B278** (1992) 187.

[33] K. Cheung, *Phys. Rev.* **D48** (1993) 1035.

[34] O.J.P. Eboli and M.C. Gonzales-Garcia, *Phys. Rev.* **D49** (1994) 91.

[35] Proceedings of the “*HERA Workshop*”, ed. R.D. Peccei, Desy, Hamburg, October 1987;
 Proceedings of the “*HERA Workshop*”, eds. W. Buchmüller and G. Ingelman, Desy, Hamburg, October 1991.

[36] K.J.F. Gaemers, R.M. Godbole and M. van der Horst, in ref. [35] (1987).

[37] K. Hikasa, Particle Data Book, *Phys. Rev.* **D45** 11-II (1992).

[38] G. Grindhammer, D. Haidt, J. Ohnemus, J. Vermaseren and D. Zeppenfeld, in ref. [7].

[39] T. Han and C. Liu, *Z. Phys.* **C28** (1985) 295;
 D.A. Dicus and S. Willenbrock, *Phys. Rev.* **D32** (1985) 1642.

[40] J. Blumlein, G.J. van Oldenborgh and R. Ruckl, *Nucl. Phys.* **B395** (1993) 35.

[41] K. Cheung, *Phys. Lett.* **B319** (1993) 244.

[42] B. Grzadkowski, S. Pokorski and J. Rosiek, *Phys. Lett.* **B272** (1991) 143.

[43] R. Kleiss and W.J. Stirling, *Nucl. Phys.* **B262** (1985) 235.

[44] C. Mana and M. Martinez, *Nucl. Phys.* **B287** (1987) 601.

[45] K. Hagiwara and D. Zeppenfeld, *Nucl. Phys.* **B274** (1986) 1.

[46] P.N. Harriman, A.D. Martin, R.G. Roberts and W.J. Stirling, *Phys. Rev.* **D42** (1990) 798.

[47] A.D. Martin, R.G. Roberts and W.J. Stirling, *Phys. Rev.* **D50** (1994) 6734.

[48] G.P. Lepage, *Jour. Comp. Phys.* **27** (1978) 192.

[49] V. Telnov, *Nucl. Instrum. Methods* **A294** (1990) 72;
 I. Ginzburg, G. Kotkin, V. Serbo and V. Telnov, *Nucl. Instrum. Methods* **A205** (1983) 47, **A219** (1984) 5.

- [50] CDF Collaboration, F. Abe *et al.*, *Phys. Rev.* **D50** (1994) 2966; *Phys. Rev. Lett.* **73** (1994) 225.
- [51] Z. Kunszt and W.J. Stirling, in ref. [7];
P.M. Zerwas, in ref. [22].
- [52] T. Stelzer and W.F. Long, *Comp. Phys. Comm.* **81** (1994) 357.
- [53] E. Murayama, I. Watanabe and K. Hagiwara, HELAS: HELicity Amplitude Subroutines for Feynman Diagram Evaluations, *KEK Report* 91-11, January 1992.
- [54] U. Baur and J.J. Van der Bij, *Nucl. Phys.* **B304** (1988) 451.
- [55] ATLAS Technical Proposal, CERN/LHC/94-43 LHCC/P2, December 1994.
- [56] CMS Technical Proposal, CERN/LHC/94-43 LHCC/P1, December 1994.
- [57] G. Abu Leil and S. Moretti, *preprint* DFTT 62/94, DTP/94/108, July 1995.
- [58] S. Moretti, *Phys. Rev.* **D50** (1994) 2016.

Table Captions

Tab. I Production cross sections for processes (1)–(3), at $\sqrt{s}_{ep} = 1.36$ TeV, with $M_\phi = 60, 80, 100, 120$ and 140 GeV. The HMRS(B) structure functions are used. The errors are the statistical errors on the numerical calculation.

Tab. II Production cross sections for processes (1)–(3) in (a)–(c), respectively, at $\sqrt{s}_{ep} = 1.36$ TeV, with $M_\phi = 60$ GeV, for all different flavour combinations entering in the partonic subprocesses. The HMRS(B) structure functions are used. The errors are the statistical errors on the numerical calculation.

Tab. III Production cross sections for the background processes discussed in the text. The HMRS(B) structure functions are used. The errors are the statistical errors on the numerical calculation.

Tab. IV Number of signal (S) and background events (B) and their statistical significance (S/\sqrt{B}), for the processes (1)–(3), at $\sqrt{s}_{ep} = 1.36$ TeV, in the window $|M_{b\bar{b}} - M_\phi| < 5$ GeV, for the usual selection of Higgs masses. Numbers correspond to hadronic(leptonic) decays of the W^\pm/Z^0 's. The HMRS(B) structure functions are used. The symbol “–” indicates the case in which the backgrounds do not constitute a problem in disentangling the signals.

Tab. V Total number of signal (S_{tot}) and background events (B_{tot}) and their statistical significance ($S_{\text{tot}}/\sqrt{B_{\text{tot}}}$), after summing the numbers in tab. IV in “inclusive” rates.

Tab. VI \mathcal{SM} Higgs boson \mathcal{H} -couplings to the gauge bosons W^\pm and Z^0 .

Tab. VII \mathcal{SM} right and left handed couplings (c_R, c_L) of u - and d -type quarks to the neutral gauge bosons g, γ, Z^0 , to the charged W^\pm 's and to the Higgs boson ϕ . We have $g_R^q = -Q^q s_W^2$ and $g_L^q = T_3^q - Q^q s_W^2$ ($q = u, d$), with $(Q^u, T^u) = (+\frac{2}{3}, \frac{1}{2})$ and $(Q^d, T_3^d) = (-\frac{1}{3}, -\frac{1}{2})$ for quark charges and isospins.

Figure Captions

Fig. 1 Feynman diagrams contributing in lowest order to $q\gamma \rightarrow q'V\phi$, where $q(q')$ represents a quark, $V(V^*)$ an external(internal) vector boson and ϕ the \mathcal{SM} Higgs boson, in the unitary gauge. In the case $V = Z^0$ and $q' = q$ only the first eight diagrams of fig. 1 contribute.

Fig. 2 Feynman diagrams contributing in the lowest order to $g\gamma \rightarrow q\bar{q}\phi$, where q represents a quark and ϕ the \mathcal{SM} Higgs boson, in the unitary gauge.

Fig. 3 Cross sections of process (1) as a function of \sqrt{s}_{ep} , for a selection of Higgs masses. The HMRS(B) structure functions are used.

Fig. 4 Cross sections of process (2) as a function of \sqrt{s}_{ep} , for a selection of Higgs masses. The HMRS(B) structure functions are used.

Fig. 5 Cross sections of process (3) as a function of \sqrt{s}_{ep} , for a selection of Higgs masses. The HMRS(B) structure functions are used.

Fig. 6 Differential distributions in the invariant mass of the $b\bar{b}$ -pair $M_{b\bar{b}}$ for the $\bar{t}bX \rightarrow b\bar{b}W^\pm X$ and $t\bar{t}X \rightarrow b\bar{b}W^\pm X$ backgrounds, at $\sqrt{s}_{ep} = 1.36$ TeV. The HMRS(B) structure functions are used.

Fig. 7 Differential distributions in the invariant mass of the $b\bar{b}$ -pair $M_{b\bar{b}}$ for the $\bar{t}bX \rightarrow b\bar{b}W^\pm X$ and $t\bar{t}X \rightarrow b\bar{b}W^\pm X$ backgrounds, at $\sqrt{s}_{ep} = 1.36$ TeV, after the cut $|M_{bW \rightarrow bjj} - m_t| > 15$ GeV. The HMRS(B) structure functions are used.

Fig. 8 Differential distributions in the invariant mass of the bW -system M_{Wb} for the $\bar{t}bX \rightarrow b\bar{b}W^\pm X$ and $t\bar{t}X \rightarrow b\bar{b}W^\pm X$ backgrounds, and the signal $W^\pm \phi X \rightarrow W^\pm (b\bar{b})X$ with $M_\phi = 60, 140$ GeV, at $\sqrt{s}_{ep} = 1.36$ TeV. The HMRS(B) structure functions are used.

σ (fb)			
M_ϕ (GeV)	$q'W^\pm\phi$	$qZ^0\phi$	$q\bar{q}\phi$
60	55.61 ± 0.34	6.13 ± 0.10	3.806 ± 0.058
80	42.84 ± 0.25	3.056 ± 0.052	1.765 ± 0.029
100	34.53 ± 0.14	1.581 ± 0.028	0.872 ± 0.013
120	27.56 ± 0.11	0.798 ± 0.024	0.4513 ± 0.0068
140	22.048 ± 0.080	0.547 ± 0.018	0.2419 ± 0.0039
$\sqrt{s} = 1.36$ TeV		HMRS(B)	

Table I

Flavours	σ (fb)
$u\gamma \rightarrow dW^+\phi + \bar{u}\gamma \rightarrow \bar{d}W^-\phi$	29.58 ± 0.15
$d\gamma \rightarrow uW^-\phi + \bar{d}\gamma \rightarrow \bar{u}W^+\phi$	19.37 ± 0.30
$s\gamma \rightarrow cW^-\phi + \bar{s}\gamma \rightarrow \bar{c}W^+\phi$	4.228 ± 0.021
$c\gamma \rightarrow sW^+\phi + \bar{c}\gamma \rightarrow \bar{s}W^-\phi$	1.620 ± 0.012
$b\gamma \rightarrow tW^-\phi + \bar{b}\gamma \rightarrow \bar{t}W^+\phi$	0.7995 ± 0.0033
$\sqrt{s} = 1.36$ TeV HMRS(B) $M_\phi = 60$ GeV	

Table IIa

Flavours	σ (fb)
$u\gamma \rightarrow uZ^0\phi + \bar{u}\gamma \rightarrow \bar{u}Z^0\phi$	4.535 ± 0.097
$d\gamma \rightarrow dZ^0\phi + \bar{d}\gamma \rightarrow \bar{d}Z^0\phi$	0.982 ± 0.025
$s\gamma \rightarrow sZ^0\phi + \bar{s}\gamma \rightarrow \bar{s}Z^0\phi$	0.2707 ± 0.0015
$c\gamma \rightarrow cZ^0\phi + \bar{c}\gamma \rightarrow \bar{c}Z^0\phi$	0.3018 ± 0.0012
$b\gamma \rightarrow bZ^0\phi + \bar{b}\gamma \rightarrow \bar{b}Z^0\phi$	0.03839 ± 0.00017
$\sqrt{s} = 1.36 \text{ TeV}$ HMRS(B) $M_\phi = 60 \text{ GeV}$	

Table IIb

Flavours	σ (fb)
$g\gamma \rightarrow u\bar{u}\phi$	$(60.4 \pm 2.2) \times 10^{-6}$
$g\gamma \rightarrow d\bar{d}\phi$	$(51.09 \pm 0.83) \times 10^{-6}$
$g\gamma \rightarrow s\bar{s}\phi$	$(11.113 \pm 0.071) \times 10^{-3}$
$g\gamma \rightarrow c\bar{c}\phi$	0.6572 ± 0.0025
$g\gamma \rightarrow b\bar{b}\phi$	0.5188 ± 0.0019
$g\gamma \rightarrow t\bar{t}\phi$	2.6192 ± 0.0049
$\sqrt{s} = 1.36$ TeV HMRS(B) $M_\phi = 60$ GeV	

Table IIc

Background	σ (fb)
$ep \rightarrow W^\pm Z^0 X$	224.3 ± 1.9
$ep \rightarrow \bar{t}bX \rightarrow b\bar{b}W^\pm X$	535.3 ± 5.1
$ep \rightarrow t\bar{t}X \rightarrow b\bar{b}W^\pm X$	1114.7 ± 1.4
$ep \rightarrow Z^0 Z^0 X$	12.15 ± 0.50
$ep \rightarrow q\bar{q}Z^0 X$	3714 ± 91
$\sqrt{s} = 1.36$ TeV HMRS(B)	

Table III

Process	S	B	S/\sqrt{B}	M_ϕ (GeV)
$q'W^\pm\phi$	99(42)	418(179)	4.84(3.14)	
$qZ^0\phi$	11(2)	0(0)	$-(-)$	60
$q\bar{q}\phi$	10	0	—	
$q'W^\pm\phi$	75(32)	452(194)	3.53(2.30)	
$qZ^0\phi$	5(1)	0(0)	$-(-)$	80
$q\bar{q}\phi$	4	0	—	
$q'W^\pm\phi$	59(25)	412(177)	2.91(1.88)	
$qZ^0\phi$	3(0)	0(0)	$-(0)$	100
$q\bar{q}\phi$	2	196	0.14	
$q'W^\pm\phi$	41(17)	357(153)	2.17(1.37)	
$qZ^0\phi$	1(0)	0(0)	$-(0)$	120
$q\bar{q}\phi$	1	0	—	
$q'W^\pm\phi$	18(8)	300(128)	1.10(0.71)	
$qZ^0\phi$	0(0)	0(0)	0(0)	140
$q\bar{q}\phi$	0	0	0	

Table IV

S_{tot}	B_{tot}	$S_{\text{tot}}/\sqrt{B}_{\text{tot}}$	M_ϕ (GeV)
120(44)	418(179)	5.87(3.32)	60
84(33)	452(194)	3.95(2.37)	80
64(26)	608(373)	2.60(1.35)	100
43(18)	357(153)	2.28(1.46)	120
19(8)	300(128)	1.10(0.71)	140

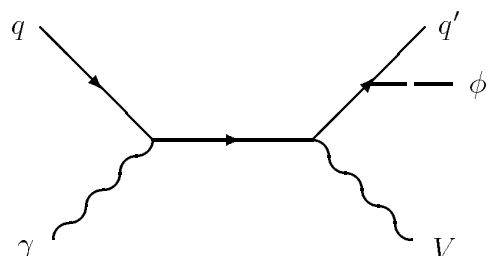
Table V

	ϕ
$W^\pm W^\mp$	$\frac{M_{W^\pm}}{s_W}$
$Z^0 Z^0$	$\frac{M_{W^\pm}}{s_W c_W^2}$

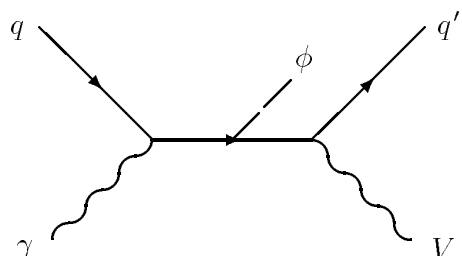
Table VI

g	γ	Z^0	W^\pm	ϕ
(1, 1)	$Q^q(1, 1)$	$\frac{1}{s_W c_W}(g_R^q, g_L^q)$	$\frac{1}{\sqrt{2}s_W}(0, 1)$	$\frac{m_q}{2M_{W^\pm}s_W}(1, 1)$

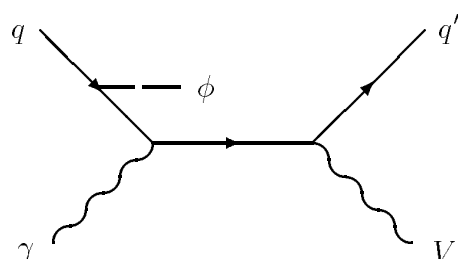
Table VII



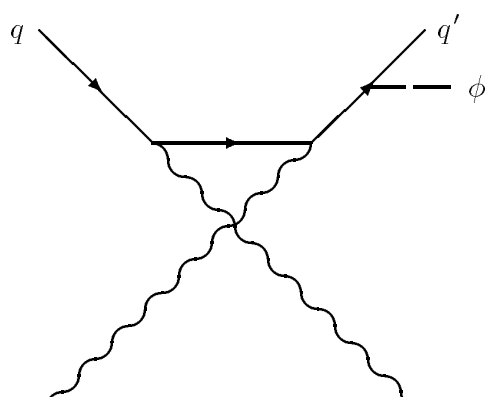
(1)



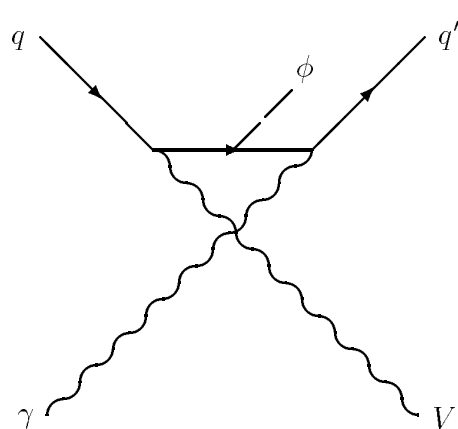
(2)



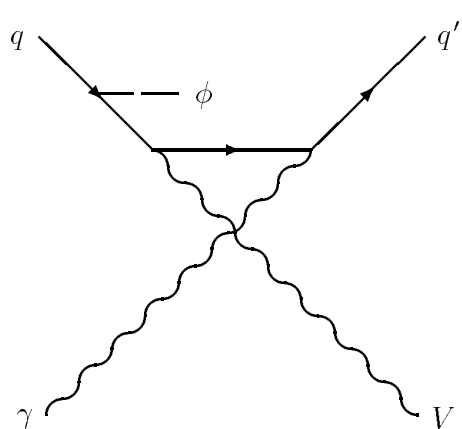
(3)



(4)

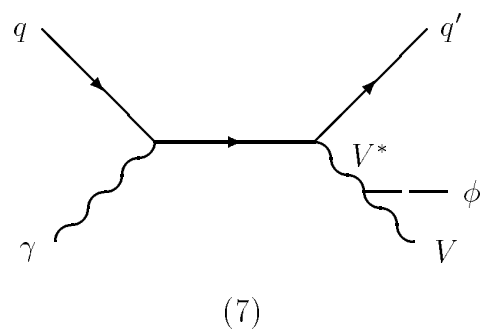


(5)

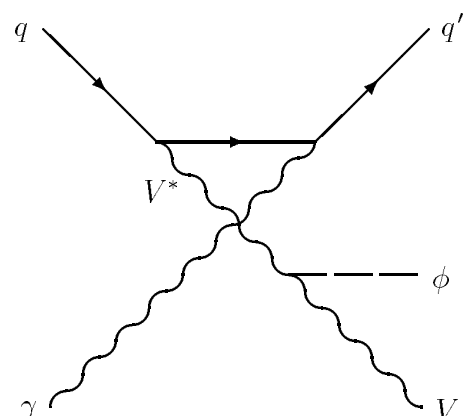


(6)

Fig. 1

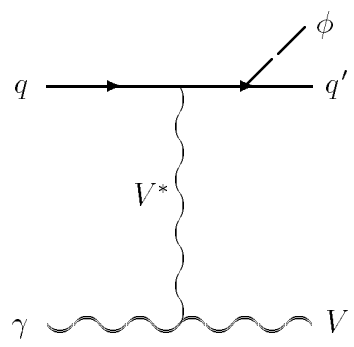


(7)

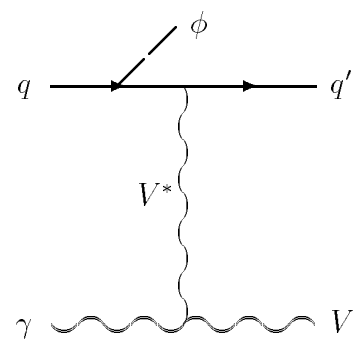


(8)

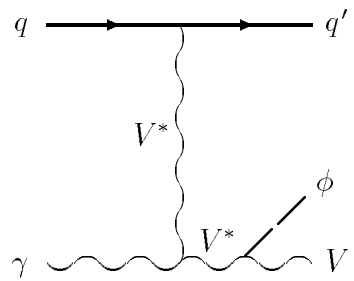
Fig. 1 (Continued)



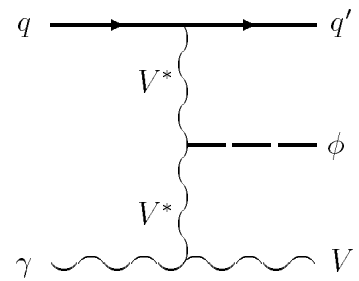
(9)



(10)



(11)



(12)

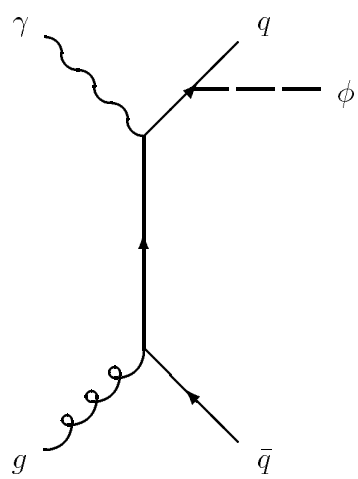
Fig. 1 (Continued)

This figure "fig1-1.png" is available in "png" format from:

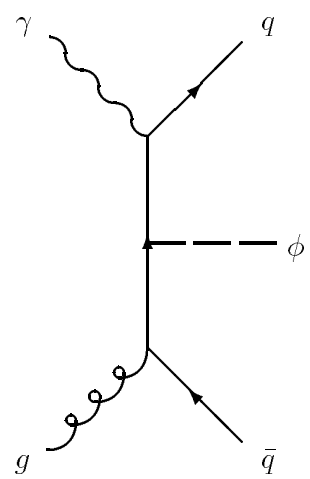
<http://arxiv.org/ps/hep-ph/9503348v2>

This figure "fig2-1.png" is available in "png" format from:

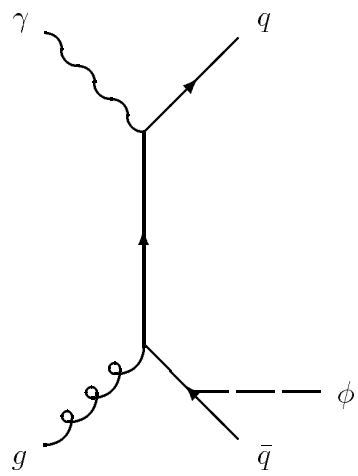
<http://arxiv.org/ps/hep-ph/9503348v2>



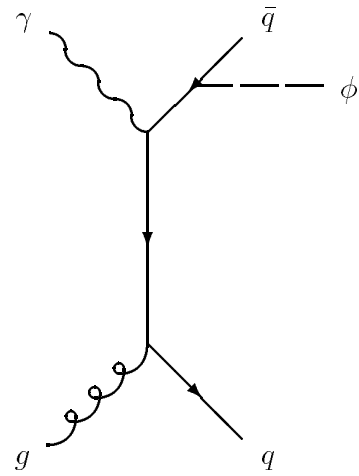
(1)



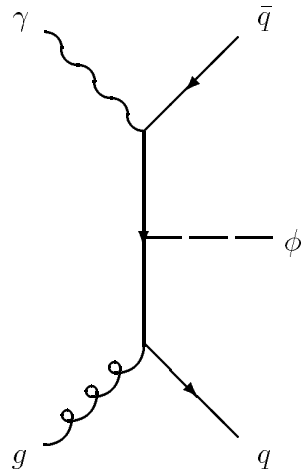
(2)



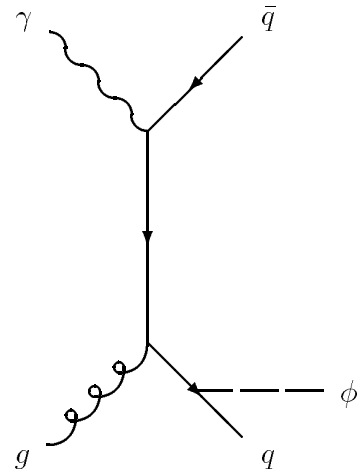
(3)



(4)



(5)



(6)

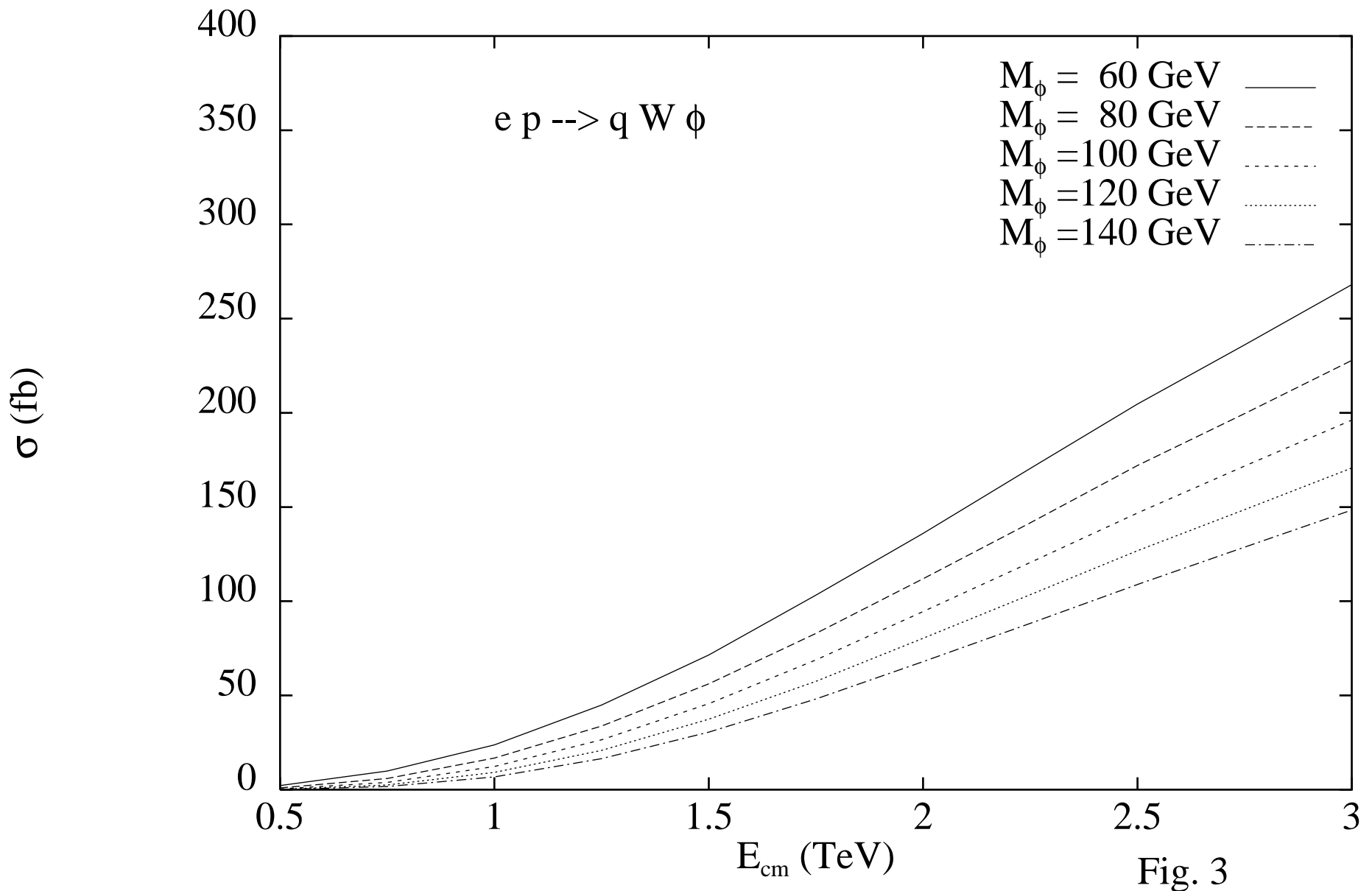
Fig. 2

This figure "fig1-2.png" is available in "png" format from:

<http://arxiv.org/ps/hep-ph/9503348v2>

This figure "fig2-2.png" is available in "png" format from:

<http://arxiv.org/ps/hep-ph/9503348v2>

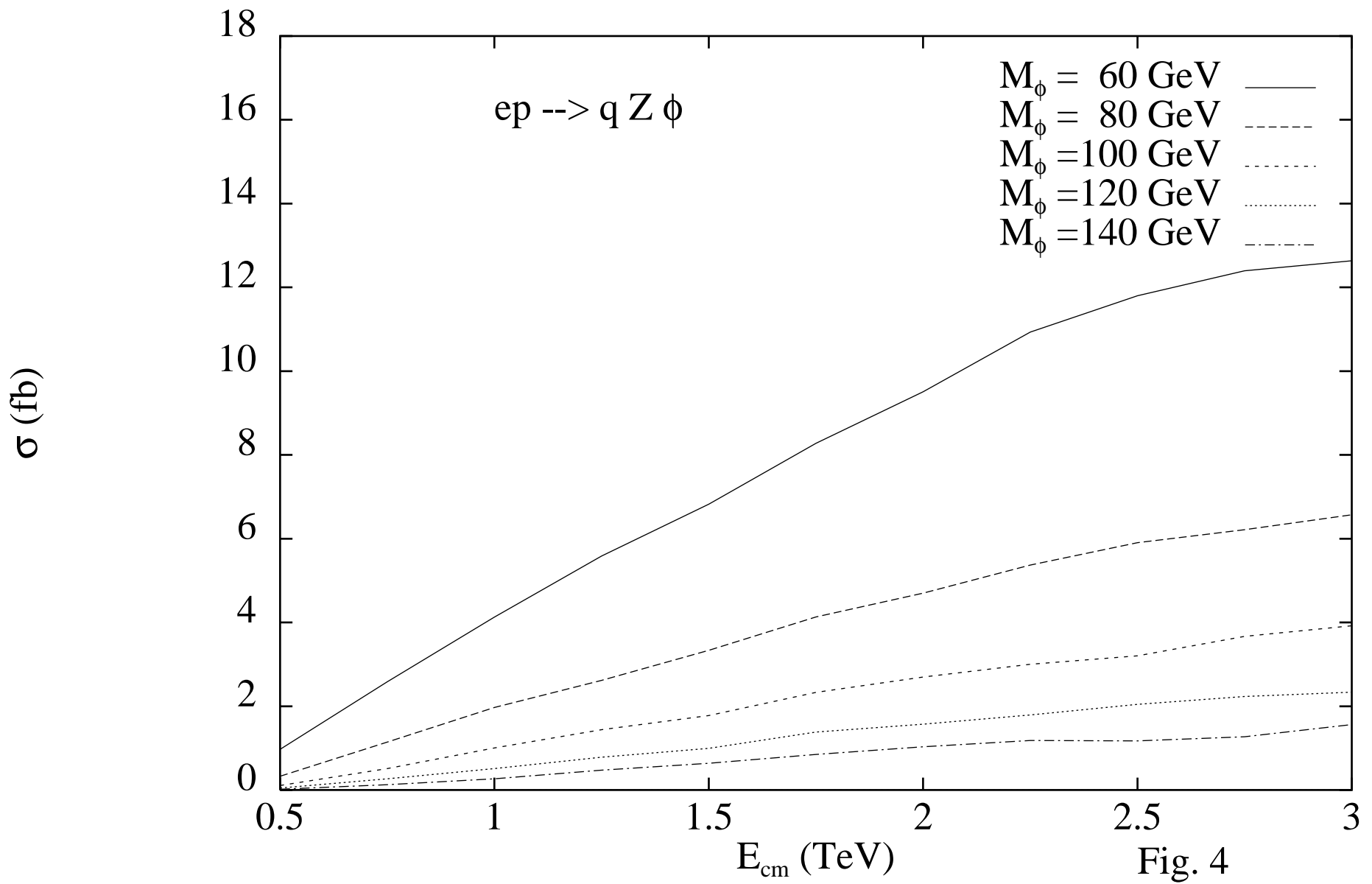


This figure "fig1-3.png" is available in "png" format from:

<http://arxiv.org/ps/hep-ph/9503348v2>

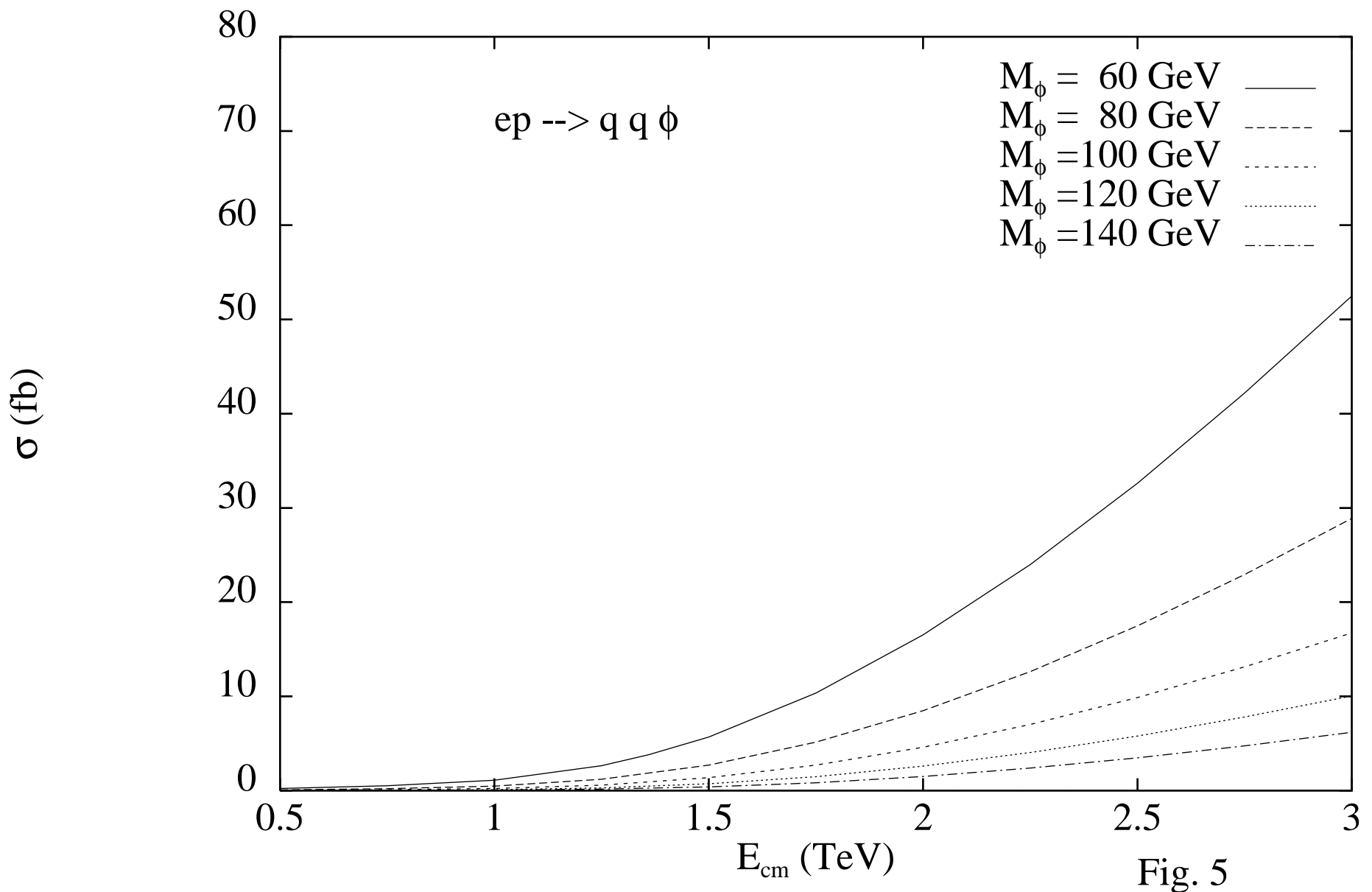
This figure "fig2-3.png" is available in "png" format from:

<http://arxiv.org/ps/hep-ph/9503348v2>



This figure "fig2-4.png" is available in "png" format from:

<http://arxiv.org/ps/hep-ph/9503348v2>



This figure "fig2-5.png" is available in "png" format from:

<http://arxiv.org/ps/hep-ph/9503348v2>

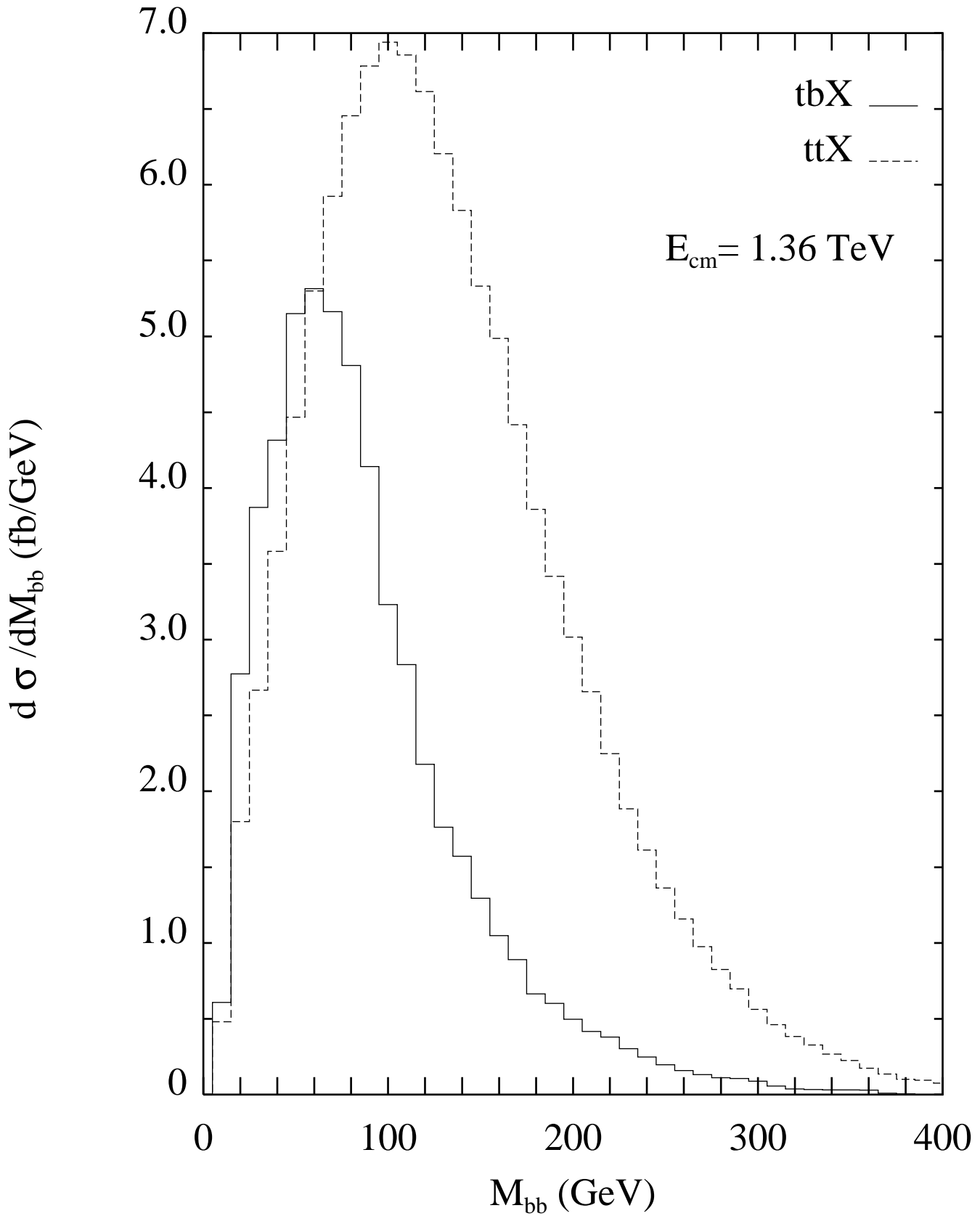


Fig. 6

This figure "fig2-6.png" is available in "png" format from:

<http://arxiv.org/ps/hep-ph/9503348v2>

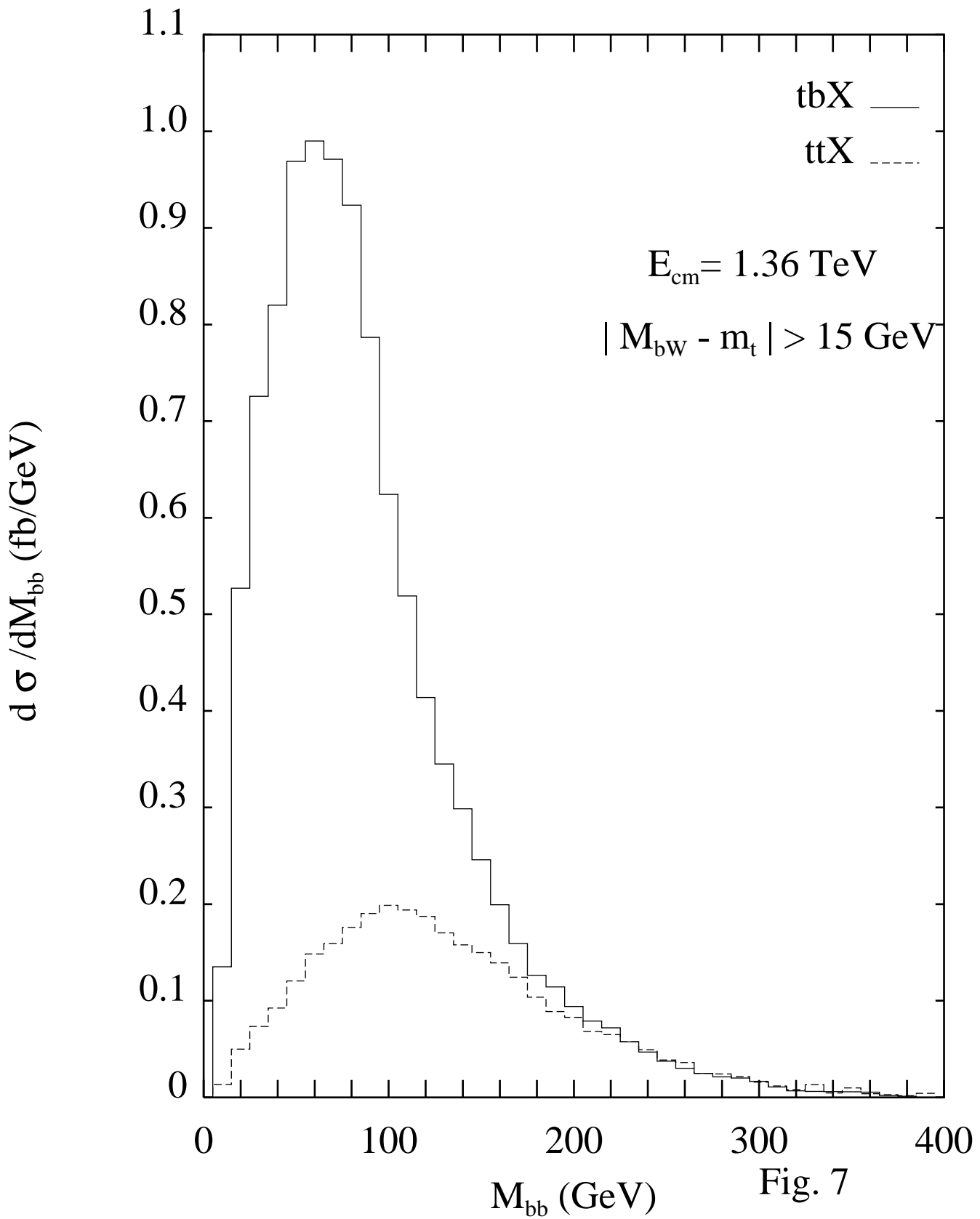


Fig. 7

This figure "fig2-7.png" is available in "png" format from:

<http://arxiv.org/ps/hep-ph/9503348v2>

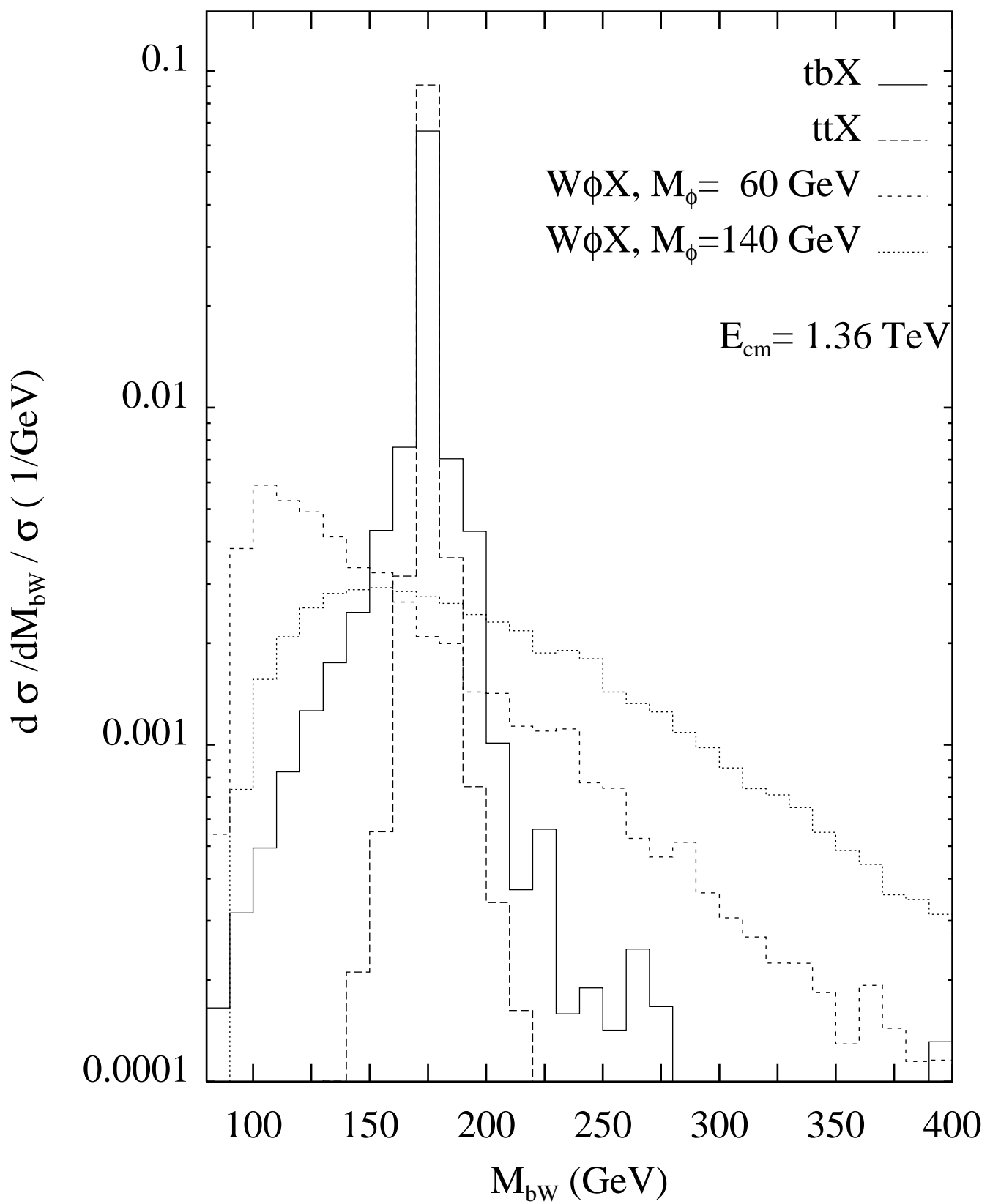


Fig. 8